THESIS

INCREASING VERTICAL RESOLUTION OF THREE - DIMENSIONAL

ATMOSPHERIC WATER VAPOR RETRIEVALS USING A NETWORK OF

SCANNING COMPACT MICROWAVE RADIOMETERS

Submitted by

Swaroop Sahoo

Department of Electrical and Computer Engineering

In partial fulfillment of the requirements

For the Degree of Master of Science

Colorado State University

Fort Collins, Colorado

Spring 2011

Master's Committee:

    Advisor: Steven. C. Reising

    V. N. Bringi
    David A. Krueger

ABSTRACT

INCREASING VERTICAL RESOLUTION OF THREE - DIMENSIONAL
ATMOSPHERIC WATER VAPOR RETRIEVALS USING A NETWORK OF
SCANNING COMPACT MICROWAVE RADIOMETERS

The thermodynamic properties of the troposphere, in particular water vapor content and temperature, change in response to physical mechanisms, including frictional drag, evaporation, transpiration, heat transfer and flow modification due to terrain. The planetary boundary layer (PBL) is characterized by a high rate of change in its thermodynamic state on time scales of typically less than one hour. Large horizontal gradients in vertical wind speed and steep vertical gradients in water vapor and temperature in the PBL are associated with high-impact weather. Observation of these gradients in the PBL with high vertical resolution and accuracy is important for improvement of weather prediction. Satellite remote sensing in the visible, infrared and microwave provide qualitative and quantitative measurements of many atmospheric properties, including cloud cover, precipitation, liquid water content and precipitable water vapor in the upper troposphere. However, the ability to characterize the thermodynamic properties of the PBL is limited by the confounding factors of ground emission in microwave channels and of cloud cover in visible and IR channels.

Ground-based microwave radiometers are routinely used to measure thermodynamic profiles. The vertical resolution of such profiles retrieved from radiometric brightness temperatures depends on the number and choice of frequency channels, the scanning strategy and the accuracy of brightness temperature measurements. In the standard technique, which uses brightness temperatures from vertically pointing radiometers, the vertical resolution of the retrieved water vapor profile is similar to or larger than the altitude at which retrievals are performed. This study focuses on the improvement of the vertical resolution of water vapor retrievals by including scanning measurements at a variety of elevation angles. Elevation angle scanning increases the path length of the atmospheric emission, thus improving the signal-to-noise ratio. This thesis also discusses Colorado State University's (CSU) participation in the European Space Agency (ESA)'s "Mitigation of Electromagnetic Transmission errors induced by Atmospheric WAter Vapor Effects" (METAWAVE) experiment conducted in the fall of 2008. CSU deployed a ground-based network of three Compact Microwave Radiometers for Humidity profiling (CMR-Hs) in Rome to measure atmospheric brightness temperatures. These measurements were used to retrieve high-resolution 3-D atmospheric water vapor and its variation with time. High-resolution information about water vapor can be crucial for the mitigation of wet tropospheric path delay variations that limit the quality of Interferometric Synthetic Aperture Radar satellite interferograms.

Three-dimensional water vapor retrieval makes use of radiative transfer theory, algebraic tomographic reconstruction and Bayesian optimal estimation coupled with Kalman filtering. In addition, spatial interpolation (kriging) is used to retrieve water

vapor density at unsampled locations. 3-D humidity retrievals from Rome data with vertical and horizontal resolution of 0.5 km are presented. The water vapor retrieved from CMR-H measurements is compared with MM5 Mesoscale Model output, as well as with measurements from the Medium Resolution Imaging Spectrometer (MERIS) aboard ESA's ENVISAT and the Moderate Resolution Imaging Spectroradiometer (MODIS) aboard NASA's Aqua and Terra satellites.

ACKNOWLEDGMENTS

TABLE OF CONTENTS

LIST OF FIGURES

LIST OF TABLES

Chapter 1

Introduction

1.1 Scientific Motivation

The planetary boundary layer (PBL) is defined as that part of the troposphere that is directly influenced by the presence of the Earth's surface and responds to physical influences from the surface within a time scale of one hour or less. These include frictional drag, evaporation, transpiration, heat transfer and flow modification due to terrain. The depth of the PBL is highly variable in both time and space [1]. The PBL is usually shallower during the night than during the day and during the winter than during the summer. These diurnal and seasonal variations are not caused by direct forcing of solar variation on the boundary layer. On the contrary, little solar radiation is absorbed by the boundary layer; most is transmitted to the ground. It is the ground that warms and cools in response to the radiation which in turn changes the boundary layer through transport processes. The entire troposphere can change in response to surface influences, but the response in the boundary layer occurs on the time scale of about one hour or so, while the response above the boundary layer takes much longer.

Turbulence is an important transport process and is used to define the PBL. Turbulence is caused by to the mean wind, which is responsible for very rapid horizontal advection. Advection refers to the transport of an atmospheric property due solely to the mass motion of the atmosphere [2]. Horizontal winds on the order of 2-10 m/s are common in the boundary layer. However, friction causes the mean wind speed to be

lowest near the ground. Vertical mean winds are usually small and on the order of millimeters to centimeters per second. This creates turbulence in the boundary layer, which leads to a PBL height that is constantly changing. The relatively high frequency of occurrence of turbulence is one of the characteristics that distinguish the boundary layer from the rest of the atmosphere. Therefore, detecting the height of the PBL and inversions in the PBL is important. An inversion of water vapor density or temperature in the troposphere is an abrupt change in that property from decreasing to increasing with altitude. Satellite remote sensing at visible or infrared wavelengths has been relatively successful in measuring variables directly associated with clouds such as cloud cover, liquid water or precipitable water. However, direct measurement of the PBL inversion characteristics, i.e., temperature or humidity inversions, has been difficult. The main reason is that to perform these measurements, satellite retrievals must have fine vertical resolution, on the order of hundreds of meters or better [3].

The height of the PBL is usually 300 m to 3 km above the Earth's surface. It is simple to determine the height of the PBL from thermodynamic profiles. The top of the PBL is often distinguished by a temperature inversion, a change in air mass, a hydrolapse, and/or a change in wind speed and/or wind direction. A hydrolapse is a marked rapid change in water vapor with height and is most well defined during differential advection, i.e. the movement of layers of the atmosphere over each other. The height of the atmospheric boundary layer and the inversion characteristics of the PBL are typically determined using radiosonde data, i.e. temperature and humidity profiles, because radiosondes measure profiles with a vertical resolution of 5-20 meters in the lower and mid troposphere, sufficient for determining boundary layer height. Water

vapor density, typically referred to as humidity in meteorology, changes with altitude. Rapid changes in water vapor density can be used to detect the top of the PBL.
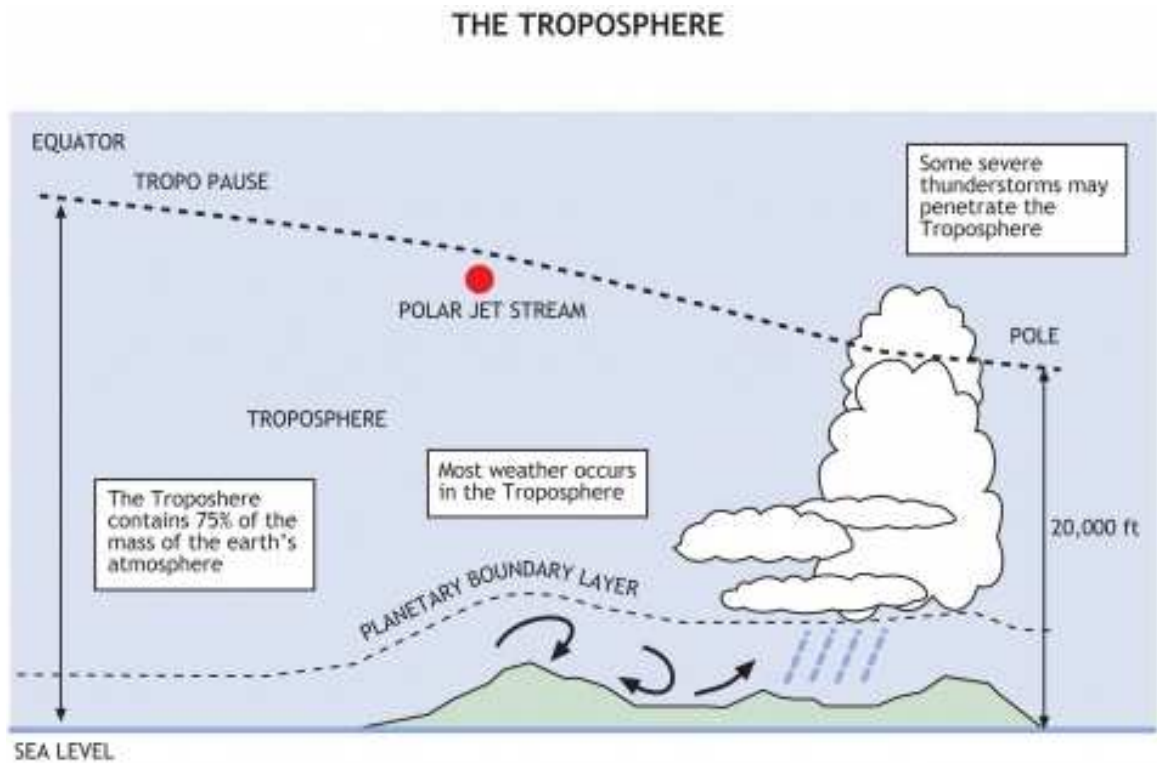
Figure 1.1. The planetary boundary layer is shown as the lowest part of the troposphere [4].

1.2 Water Vapor Profile Measurement Techniques

Methods of measuring water vapor density include in-situ instruments such as radiosondes and remote sensing instruments such as microwave radiometers and Raman lidars. The cost of a radiosonde is approximately US$200, and each one can be used only once, limiting both the horizontal sampling and temporal repeat time. In addition, sondes are often advected horizontally up to hundreds of kilometers from their launch site by the time they reach the tropopause. Raman lidars has high vertical resolution for water vapor measurement, but are expensive instruments. Under optimal conditions, they have

vertical resolution and measurement accuracy comparable to those of radiosonde measurements. The performance of these large and expensive systems, however, degrades during daylight hours, and their use is limited to clear-sky conditions.

Microwave radiometers can be used to retrieve water vapor density profiles. Commercially-available radiometers from Radiometrics are relatively large and heavy, with a mass of 25 to 30 kg and dimensions of approximately 50 x 28 x 76 cm. This

Table 1.1 shows the horizontal, vertical and temporal resolution of various ground-based and space-borne sensors.

Sensor	Horizontal Resolution (km)	Vertical Resolution (km)	Temporal Resolution	Frequency Band
Radiosonde	~ 100 (NWS)	0.01 - 0.5	12 hr (operational)	In-situ
GPS Ground-Based Network	~50	0.5 – 1 (expected)	30 min	L-Band
COSMIC satellite constellation	200	0.1 – 0.5	30 min	L-Band
AMSU-B satellite	20	2	12 hr	183 GHz
CMR-H Ground-Based Network	0.5 - 1	0.5 – 1	10 – 15 min	K-band

Table 1.1 Comparison of horizontal, vertical and temporal resolution of various remote sensing instruments

makes the deployment of radiometers in a network or their relocation somewhat difficult.

For these reasons, a low-mass, low-power radiometer called the Compact Microwave Radiometer for Humidity profiling (CMR-H) was designed and fabricated in the Microwave Systems Laboratory at Colorado State University [5]. A network of three CMR-Hs has been successfully used to retrieve water vapor profiles with a vertical resolution of 0.5 to 1.0 km [6]. To measure the planetary boundary layer height, a resolution of 0.5 km or better is required.

This thesis proposes a method for retrieving the water vapor profile with a vertical resolution of better than 500 m for the first 1 km in altitude, and better than 1 km over nearly all of the typical planetary boundary layer. The advantage of ground-based microwave radiometers is their ability to continuously monitor atmospheric water vapor in a particular volume of the atmosphere under nearly all weather conditions. Radiometers are also less expensive than most other remote sensing instruments, but their main disadvantage is lower resolution and accuracy than *in situ* instruments. Microwave radiometers have lower vertical resolution ($\sim$250 m to a few km) than radiosondes do, but they provide high-temporal resolution observations, on the order of 10 minutes. A microwave radiometer is a very sensitive receiver designed to measure thermal emission from scenes of interest, i.e. planetary surfaces and atmospheric volumes. Microwave radiometers for remote sensing measure atmospheric radiation due to Planck blackbody emission as well as its absorption and re-radiation by the atmospheric constituents along the path from the scene of interest to the sensor. The next few sections describe the atmospheric absorption models used in the retrieval of water vapor profiles.

5

1.3 Atmospheric Absorption and Emission by Gases

All gases absorb and emit electromagnetic radiation. Models of absorption and emission by gases describe the characteristics and properties (magnitude and frequency dependence, for example) of absorption lines, which are unique to each gas and are used to extract information about the composition and thermodynamic state of the atmosphere. Radiometers measure the emitted electromagnetic radiation to determine the properties of the emitter. The theory of radiative transfer describes the process of energy transfer through electromagnetic radiation.

In order to interpret atmospheric radiation measurements and to infer the state of the atmosphere, radiative transfer theory is used to describe how electromagnetic radiation interacts with gases present in the atmosphere. Absorption lines can be used to identify the composition or state of the atmosphere. Molecular absorption spectra and the shape of absorption lines are explained in the next section.

1.4 Molecular Absorption Spectra

Absorption spectra of molecules are much more complex than those of atoms. In molecules, transitions are possible not only between the energy states of the constituent atoms of the molecule but also between energy states associated with the movements of the atoms. The total internal energy ε of an isolated molecule is the sum of three energy states, as given by

$$\varepsilon = \varepsilon_e + \varepsilon_v + \varepsilon_r \tag{1.1}$$

where ε_e is the electronic energy, ε_v is the vibrational energy, and ε_r represents the rotational energy of a molecule. For each electronic state, there are a number of

associated, possible vibrational states and for each vibrational state there a number of associated, possible rotational states.

Rotational energy is due to rotational motions of the atoms of the molecule about the center of mass of the molecule. Vibrational energy is due to vibrational motions of the atoms about their equilibrium positions [7]. Figure 1.2 shows the rotation of a diatomic molecule and the vertical component of the fluctuations of the dipole in a regular mode [7]. These fluctuations are slower than those due to vibrational or electronic transitions. Figure 1.3 shows molecular absorption spectra which consists of closely spaced lines due to rotational and vibrational transitions which is known as vibration-rotation band [7] . This diagram also shows how rotational and vibrational transitions are superimposed on electronic states.
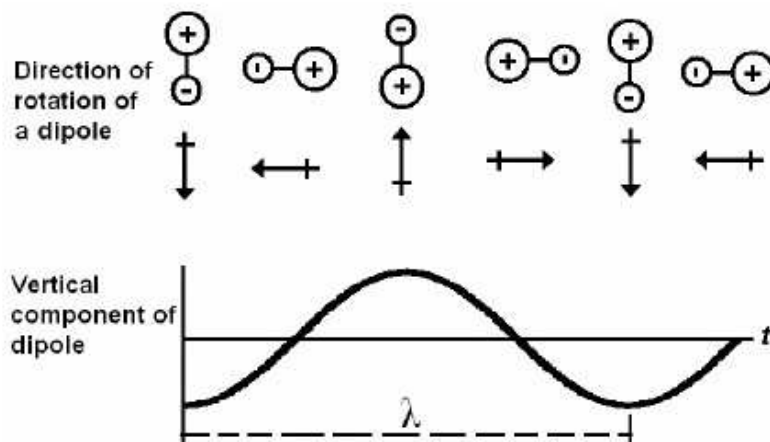
Figure 1.2. Rotation of a simple diatomic molecule, showing the fluctuation of the dipole moment measured in a particular direction [7].
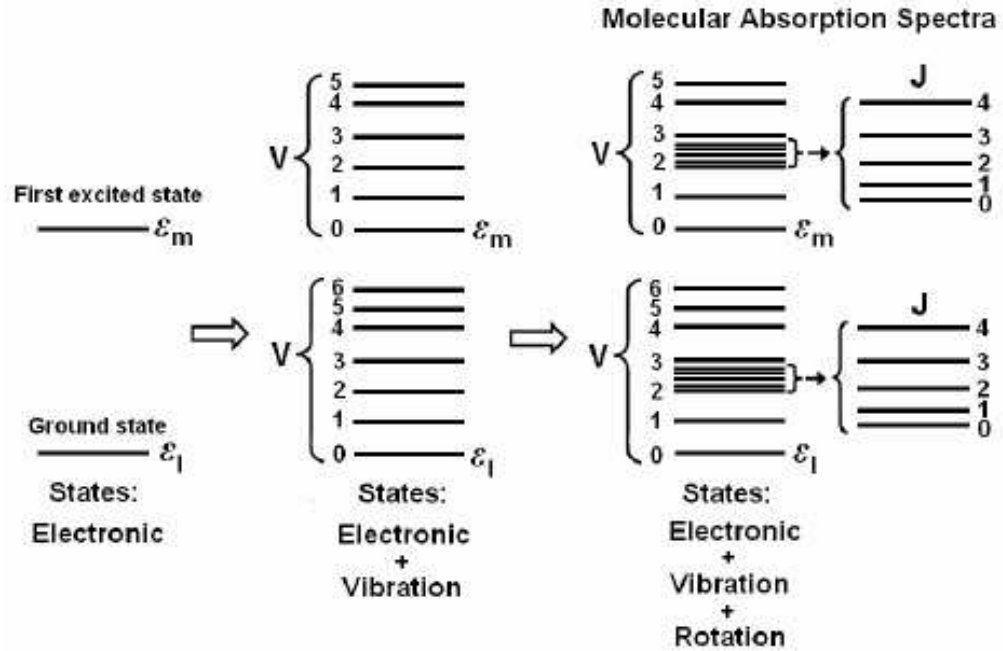
Figure 1.3. Molecular absorption spectra due to electronic, rotational and vibrational transitions. *J* and *V* are the quantum numbers associated with rotational and vibrational transitions, respectively[7].

Radiation is absorbed (or emitted) when an energy transition occurs from a lower (or higher) energy state to a higher (or lower) energy state. The frequency of the absorbed (or emitted) photon, a quantum of radiation energy, is given by

$$f_{lm} = \frac{\varepsilon_m - \varepsilon_l}{h} \qquad (1.2)$$

where h is Planck's constant and ε_m and ε_l are the internal energies of the higher and lower molecular states, respectively. The energy differences between different electronic states typically range from 2 to 10 eV (1 eV = 1.6 x 10^{-19} J). Due to the large energy differences observed during electronic transitions as compared to pure vibrational or rotational transitions, they usually result in complex band systems in the visible and ultraviolet parts of the spectrum which also involves simultaneous changes in vibrational and rotational energy states. Usually, energy differences between vibrational states vary

from about 0.1 to 2 eV. Molecules absorb radiation in the mid- and near-infrared (wavelengths between about 0.7 and 20 μm) due to vibrational transitions.

As the energy changes between purely vibrational states are several orders of magnitude higher than energy changes between purely rotational states, vibrational transitions never occur alone, but are always accompanied by many rotational transitions. This condition gives rise to a group of lines, referred to as a vibration-rotation band. Pure rotational energy transitions are usually on the order of 10^{-4} to 5×10^{-2} eV. Rotational transitions give rise to rotational lines in bands at the far-infrared wavelengths (longer than about 20 μm), extending into the microwave spectral region where individual rotational lines can be resolved.

1.5 The Shape of an Absorption Line

The previous section described the fundamentals of determining the spectral locations of absorption lines of isolated molecules. Based on Equation (1.2), the absorption (or emission) spectrum of an isolated, undisturbed, and stationary molecular system consists of sharply defined frequency lines, as shown in Figure 1.4(a), which correspond to transitions between sharply defined (quantized) energy levels of the molecule. But it is known that molecules are in constant motion, interacting and colliding with each other and with other molecular structures which result in the absorption spectrum of a gases consist of spectral lines which have significant width, as shown in Figure 1.4(b).

(a)   (b)
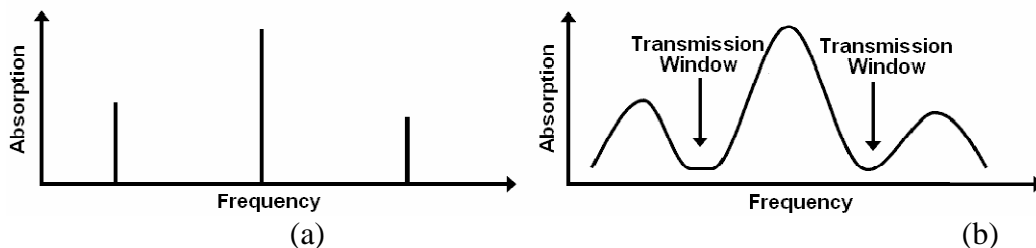
Figure 1.4. Absorption spectrum of (a) a single isolated molecule and (b) a gas containing many molecules.

This increase in line width is called *line broadening*. The spectral-line broadening relevant to the transmission of electromagnetic radiation through the gases of the Earth's lower atmosphere, particularly in the microwave region of the spectrum, results from both the individual motions of the molecules and their collisions with other molecules [8] [9]. The collisions with other molecules give rise to *pressure broadening*, which depends on molecular properties as well as velocity distribution and collision times. In a molecular system, the absorption spectrum for transitions between energy states, ε_m and ε_l, can be written

$$\kappa_a(f, f_{lm}) = \frac{4\pi f}{c} S_{lm} F(f, f_{lm}) \tag{1.3}$$

where κ_a is the absorption coefficient described in Equation (1.3), f is the absorption frequency, f_{lm} is the molecular resonance frequency, c is the velocity of light, S_{lm} is the *line strength* of the absorption spectrum, and F is the *line-shape* function, which describes the shape of the absorption spectrum with respect to the resonance frequency, f_{lm}. The line strength, S_{lm}, of a specific gas is determined by the number density of absorbing molecules, the thermodynamic temperature of the gas and the molecular parameters associated with the transition. As long as other parameters are constant, a pressure-broadened line widens as the pressure increases.

In summary, the absorption (or emission) spectrum of a gas is determined by its density, its temperature, the motions of the atoms of each molecule, the motions of the molecules and their collisions with other molecules. In particular, rotational motions of the atoms of the molecules of a gas, as well as their velocity distribution and collision

times, define the characteristics of the absorption (or emission) spectrum of a gas in the microwave region.

1.6 The Absorption Coefficient of Water Vapor Near 22 GHz

Understanding the properties of the absorption coefficients of water vapor (κ_{H2O}) in the microwave region is important to retrieve information on atmospheric water vapor, from microwave radiometer measurements. For example, microwave radiation from atmospheric water vapor is unpolarized (except in the case of propagation through rain or ice clouds). In general, the stronger the absorption, the lower the polarization difference [10]. Therefore, a microwave radiometer designed to measure atmospheric water vapor or liquid water emissions needs to measure at only a single polarization. The Van-Vleck Weisskopf line shape [11] is given as

$$k_{abs\_j}(f) = (0.3633*10^3)f^2\rho_{v\_j}\ (\frac{300}{T_j})\gamma*[[\ [\ (\frac{1}{T_j})(\frac{1}{300})^{3/2}]\ e^{\frac{644}{T_j}}[\frac{1}{(22.235\ -f)^2+\gamma^2}+\frac{1}{(22.235+f)^2+\gamma^2}]\ ]\ +6.6061$$

$$\gamma = 2.85(\frac{P_j}{1013})(\frac{300}{T_j})^{0.626}[1+0.018\frac{\rho_{v\_j}T_j}{P_j}]$$
$$(1.4)$$

where the linewidth parameter γ has units of GHz, P_j is the pressure, T_j is the temperature and ρ_{v_j} is the water vapor density at jth altitude. This relationship shows the dependence of the water vapor absorption coefficient (κ_{H2O}) on meteorological parameters P, T, and ρ_v.

The effects of pressure and temperature variations on the water vapor absorption coefficient κ_{H2O} near the 22.235 GHz water vapor absorption line were studied using Equation (1.4). For example, for a constant value of both thermodynamic temperature, T,

11

of 295 K and water vapor density, ρ_v, of 7.0 g/m^3, Figure 1.5 shows that decreasing the atmospheric pressure reduces the width and increases the strength of the water vapor absorption line, with the largest effect near the center of the 22.235 GHz absorption line.
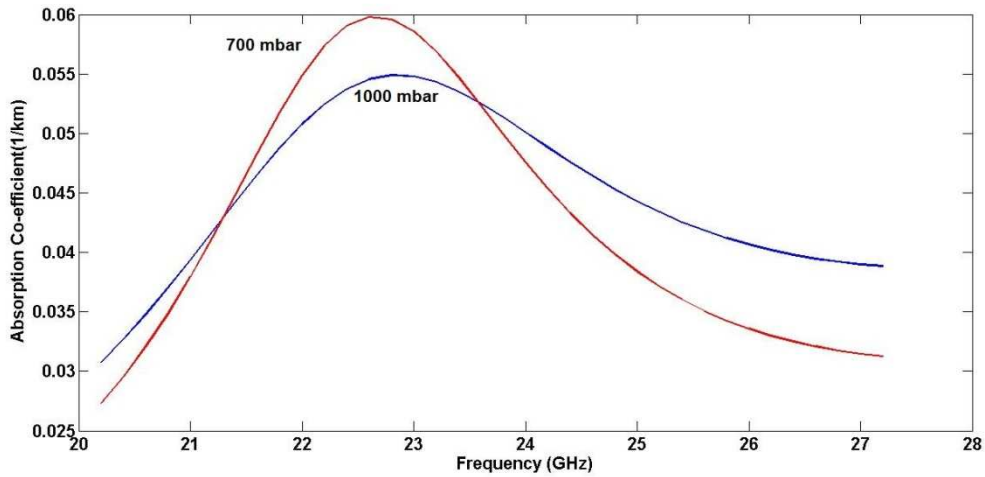
Figure 1.5. Water vapor absorption coefficient (κ_{H2O}) as a function of frequency calculated at two different atmospheric pressures for $T = 295$ K and $\rho_v = 7.0$ g/m^3.

From these results, it can be inferred that the difference between the brightness temperatures measured near the absorption line and those measured away from the absorption line increases with altitude due to the decrease in pressure with altitude.

Now, assuming a constant atmospheric pressure, P, of 1000 mbar again with a water vapor density, ρ_v, of 7.0 g/m^3, the absorption coefficient, κ_{H2O}, as a function of frequency is shown in Figure 1.6 for two different temperature values. This demonstrates that decreasing the atmospheric temperature increases both the width and the strength of the water vapor absorption line. Moreover, the sensitivity of κ_{H2O} to temperature variations increases as the frequency offset from the water vapor resonance, especially for frequencies above the resonance frequency.
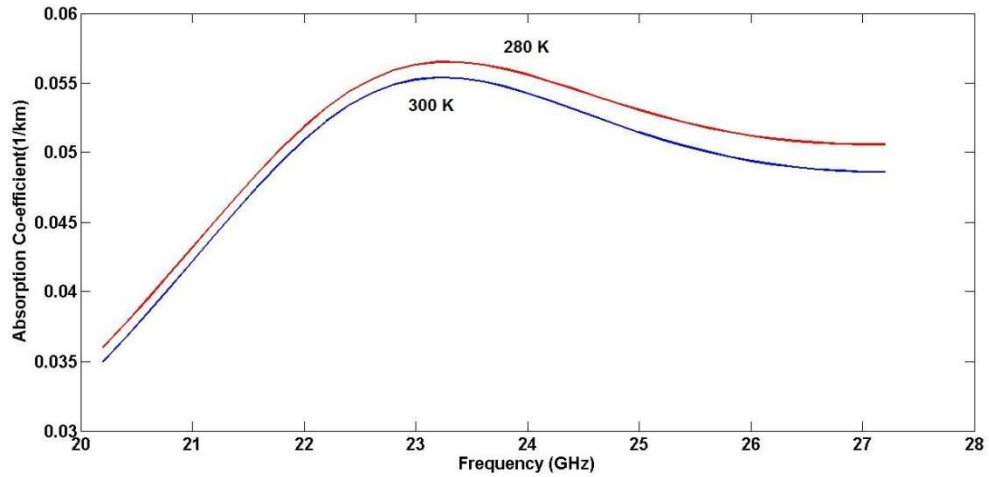
Figure 1.6. Water vapor absorption coefficient κ_{H2O} as a function of frequency calculated at different atmospheric temperatures for $P = 1000$ mbar and $\rho_v = 7.0$ g/m^3.

From comparison of Figures 1.5 and 1.6, it is evident that κ_{H2O} is more sensitive to variations in atmospheric pressure than to temperature variations, particularly at frequencies close to the water vapor resonance.

1.7 Contributions of This Thesis

The contributions of this thesis are as follows:

1) Retrieval of the 3-D water vapor field over the city of Rome from brightness temperature measurements during the Mitigation of Electromagnetic Transmission Errors induced by Atmospheric WAter Vapor Effects (METAWAVE) experiment are reported using Bayesian optimal estimation, algebraic reconstruction tomography, Kalman filtering and kriging. Comparison between the brightness temperatures measured by the CMR-H and those measured by the dual-channel radiometer deployed on the roof of La Sapienza University of Rome are presented. Integrated water vapor data retrieved from

CMR-H network data are compared with those retrieved from MODIS and MERIS instruments. The 2-D retrievals from the CMR-H network are compared with Mesoscale Model (MM5) model output.

2) A technique to increase the vertical resolution of retrieved 1-D water vapor profiles has been developed and presented using Backus-Gilbert theory, which is also discussed and presented. Brightness temperature measurements from multiple elevation angles have been used to retrieve water vapor density profiles with a vertical resolution of better than 400 meters.

3) This thesis discusses a new concept for the implementation of high vertical resolution 3-D water vapor density retrieval techniques from a network of ground-based radiometers.

1.8 Summary of Following Chapters

This thesis will discuss the results of the Mitigation of Electromagnetic Transmission Errors induced by Atmospheric Water Vapor Effects (METAWAVE) experiment as well as a technique to increase the vertical resolution of the retrieved 3-D water vapor density field.

I) Background and Related Work - Chapter 2

1) Describes recent work on water vapor density retrievals from microwave brightness temperature measurements, focusing on spatial resolution and accuracy, including the use of 3-D tomographic inversion

2) Analyzes the potential for improving the spatial resolution of retrievals and the utility of retrieved water vapor to initialize and constrain high-resolution (sub-km) numerical weather prediction models

II) Details of the METAWAVE experiment - Chapter 3

3-D water vapor retrievals as part of the METAWAVE experiment

1) Scientific background of the METAWAVE experiment

2) Measurements using a three-radiometer network of scanning Compact Microwave Radiometers for Humidity profiling (CMR-Hs) during the METAWAVE experiment

3) Retrievals of the 3-D atmospheric water vapor field using microwave brightness temperatures measured by the CMR-H network during the METAWAVE experiment

2-D and 3-D water vapor density fields retrieved from the CMR-H network measurements

- Comparison of 2-D water vapor density retrieved from CMR-H measurements with Mesoscale Model (MM5) model output. Comparison of integrated water vapor (IWV) from CMR-H network with retrievals from measurements by the MOderate Resolution Imaging Spectroradiometer (MODIS) aboard NASA's Aqua and Terra satellites and the MEdium Resolution Imaging Spectrometer (MERIS) aboard ESA's ENVISAT.

- Time series of 3-D water vapor density results from CMR-H network measurements

III) Improving vertical resolution of 1-D retrieval technique - Chapter 4

IV) This chapter will discuss a method to retrieve water vapor density profiles with improved vertical resolution of better than 500 meters. The method is:

1) Description of Backus-Gilbert theory [12]

2) Implementation of Backus-Gilbert theory using weighting functions and averaging kernels, which are linear combinations of the weighting functions

3) Minimization of the spread of averaging kernels in order to increase the vertical resolution

4) Analysis of the effect of the number of elevation angles measured on the vertical resolution

IV) Observation System Simulation Experiment (OSSE) – Chapter 5

Verifying increased vertical resolution of 1-D water vapor density retrievals using a scanning radiometer.

1) The use of simulated brightness temperatures computed from radiosonde data using the radiative transfer equation. These brightness temperatures are then used to retrieve a 1-D water vapor density profile.

2) Retrieval process using brightness temperatures measured by one scanning radiometer observing at multiple elevation angles

3) Use of the Gauss-Newton iteration method to improve vertical resolution

4) Sensitivity of the retrieval technique to variations in the error covariance matrices, including the following:

- Measurement error

- Error of the *a-priori* water vapor density

i) Scale height of the *a-priori* co-variance matrix

          ii)   Variance of the *a-priori* water vapor densities

V)   Conclusions and Future Work Chapter 6

Future work includes:

1) Increasing the retrieval accuracy, precision and temporal resolution of the retrieval of the 3-D atmospheric water vapor field.

2) A field deployment of the CMR-H network in conjunction with other water vapor remote or in-situ measurement instruments (including a Radiometrics radiometer, Raman lidar, radiosonde, etc.) observing the same volume of the atmosphere at the same time. The results from the CMR-H network can be validated through comparison with measurements from other instruments.

Chapter 2

Background and Related Work

2.1 High-Resolution Water Vapor Density Profiles

As discussed in Section 1.2, high spatial and temporal resolution information on water vapor can be very useful for NWP model initialization. In addition, high vertical resolution atmospheric water vapor density profiles can be used to detect inversions and hence the determine boundary layer height. An inversion is a layer where the normal temperature profile (warm air below, cold air above) or water vapor profile is reversed, creating a stable configuration of denser, cooler air below lighter, warmer air. An inversion exists at the top of the boundary layer.

Water vapor is the most dynamic component of the boundary layer and of the entire troposphere as well. It has been observed that total precipitable water can change by as much as 50% on a time scale of a few hours [13], even under clear-sky conditions with nearly constant surface moisture content. In contrast, the maximum variation in average atmospheric temperature at a given location over one year is about 15% [13]. Nearly all of the water vapor in the atmosphere is in the lowest 10 km of the troposphere. Water vapor influences almost all atmospheric processes, from radiative heating affecting climate on synoptic scales to local hydrological budgets as well as severe weather

conditions. Because of the large variability of water vapor and temperature, observations of temperature and humidity profiles of high accuracy, spatial and temporal resolution are needed for direct assimilation into NWP and nowcasting models. Despite the importance of water vapor density observations for forecasting quantitative precipitation, present water vapor measurement techniques have insufficient spatial and temporal resolution. This lack may limit weather forecasting because tropospheric water vapor content varies by three orders of magnitude. A 1% variation in total precipitable water within and around a storm cell has a significant and measurable effect on storm intensity [14] [15].

The variation in water vapor above the convective boundary layer directly affects the entrainment and vertical velocity within a convective storm [14] [15]. Entrainment is an atmospheric phenomenon in which a turbulent flow captures a non-turbulent flow. It is typically used to describe the capture of wind with high moisture content, or the capture of drier air by turbulent air. Entrainment can include the mixing of environmental air into a previously-existing air current or cloud so that the environmental air becomes part of the current or cloud. Therefore, sensing atmospheric water vapor is a major area of interest to NOAA, NASA, and NCAR because of the role it plays in controlling the earth's radiation budget as well as in predicting the location and intensity of small-scale convective storms. Consequently, a significant amount of work has been performed to develop systems and techniques for measurement of atmospheric water vapor, as well as to increase the spatial and temporal resolution of observed water vapor density profiles. Some of this work is summarized in the following sections.

Historically, initialization of weather prediction models depended on balloon-borne sensors, i.e., radiosondes, for observations of water vapor, temperature, pressure

and wind speed. As discussed in Section 1.2, radiosondes have very fine vertical resolution but poor horizontal resolution since they are launched from U.S. National Weather Service stations separated by an average of about 100 km in the U.S. Partly due to their poor horizontal resolution, ground-based radiometers have been used to complement radiosondes. In this chapter, various retrieval methods to obtain 1-D, 2-D 3-D water vapor density fields from ground-based radiometer measurements will be discussed. The vertical and horizontal spatial resolution of these various methods as well as their accuracy is presented.

2.2 1-D Water Vapor Profile Retrieval using Ground-Based Radiometers

Various methods have been developed to retrieve 1-D water vapor profiles from radiometer brightness temperature measurements in the last few decades, including statistical profile inversion [11] and the variational method. In statistical profile inversion, a relationship between radiometric measurements and temporally and spatially coincident radiosonde profiles is established for a particular area. Using this relationship, measured brightness temperatures can be extrapolated to retrieve water vapor and temperature profiles. The problem with this process is the anomalous estimation of profiles different from the actual profile, causing the retrieved proflies to have a negative or positive bias. Therefore, the variational method of retrieving water vapor and temperature profiles was developed. This technique uses measurements from a zenith pointing radiometer. For example, a Radiometrics profiling radiometer has 12 channels out of which five are in the 22–30 GHz band to provide water vapor profile and liquid water information and seven are in the 51–59 GHz band to determine the temperature profile. In this method a forward model is used to relate the state vector (temperature,

water vapor profile and cloud liquid) to the observation vector (brightness temperatures measured at the frequencies of operation of the channels [16]). The retrieval of temperature and humidity profiles from passive ground-based radiometers is an *ill-posed* problem because there are a large number of atmospheric states that can produce a given measurement vector within its uncertainty. This problem is addressed by the addition of background data or *a-priori* data, sometimes in the form of a short-term forecast from a NWP model [16]. This is also known as an *optimal* method of combining observations with the background data, which takes into account the error of both the observations and the background data. Therefore, this retrieval method is typically called *optimal estimation* of water vapor and temperature profiles. The optimum profile is retrieved by adjusting the atmospheric state vector in order to minimize a cost function [17] using the Levenberg–Marquardt method.

2.2.1 Vertical Resolution of Retrieved Water Vapor Profiles

Vertical resolution is an important characteristic of retrieved water vapor profiles because it gives information about the fine changes in the water vapor density profiles. The vertical resolution of the variational method can be estimated by calculating the multiplicative inverse of the elements of the main diagonal of the averaging kernel matrix [17]. As shown in Figure 2.1, the vertical resolution of temperature profiles decreases with height from approximately 700 m near the ground approximately as twice the height from 0.5 to 4 km. Similarly the vertical resolution of humidity profiles is shown as the natural log of humidity in Figure 2.1. The accuracy of water vapor profile degrades very

rapidly above 1.6 km above ground level [16]. In both the cases, vertical resolution of profiles from radiometers are poorer than those of radiosondes.
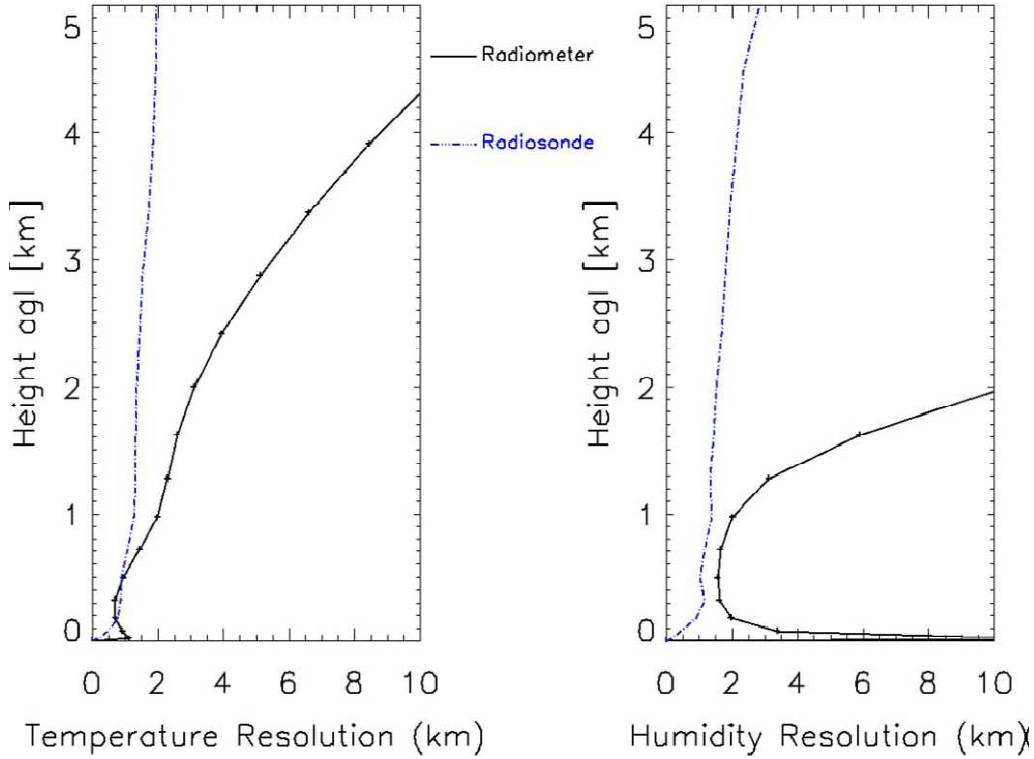
Figure 2.1. Vertical resolution of temperature and humidity (ln *q*) for radiosonde and 1D-VAR radiometer retrievals in clear U.S. standard atmosphere calculated using the averaging kernel matrix method [17].

2.3 Two-dimensional Absorption Coefficient Structure using a Scanning Radiometer

Retrieval of 1-D water vapor and temperature profiles were discussed in Section 2.2. The retrieval of 2-D absorption coefficient structure using a radiometer is discussed in the current section. The retrieval of the structure of the atmospheric specific absorption coefficient makes use of tomographic measurements. In this example, a radiometer with a single frequency channel at 23.8 GHz was used for the experiment. The radiometer

scanned a vertical plan of the atmosphere using 12 different elevation angles from 23^0 to 90^0. Tomography works best when all angles of view are available. But for this study the angular coverage is limited to a portion of the first quadrant [18]. The scanned region is modeled as a panel of 9 km height and 23 km horizontal extent. The observed region is subdivided into rectangular bins, as shown in Figure.2.2. The size of bins is smaller near the radiometer and is larger further from the radiometer. The number of elevation angles (12 in this case) was determined by the eigenstructure of the forward problem as determined by singular value decomposition (SVD) [19]. For each of the 12 elevation angles, the contribution of each bin to the brightness temperature is computed assuming that the medium properties are constant within the bin. To retrieve the absorption coefficients in each bin, the forward model is defined by linearizing the radiative transfer equation about a reference model, which also serves as the *a-priori* knowledge of the observed scene. Linearization leads to a forward model in which variations in brightness temperature about the reference model are related to variations in absorption coefficient in each bin by means of a Jacobian matrix. The problem is ill-posed because the number of measurements is less than the number of bins in which the absorption coefficient needs to be retrieved. The retrieval of absorption coefficients requires the inversion of an equation involving the rectangular Jacobian matrix. The method of least squares is used to retrieve the absorption coefficient profiles. Each scan has been designed to retrieve the 2-D structure of the atmospheric specific absorption coefficient in the scanning plane. The vertical resolution is 1.5 km, while the horizontal sizes of the bins vary from 0.5 km near the radiometer to 6 km furthest away from the radiometer.
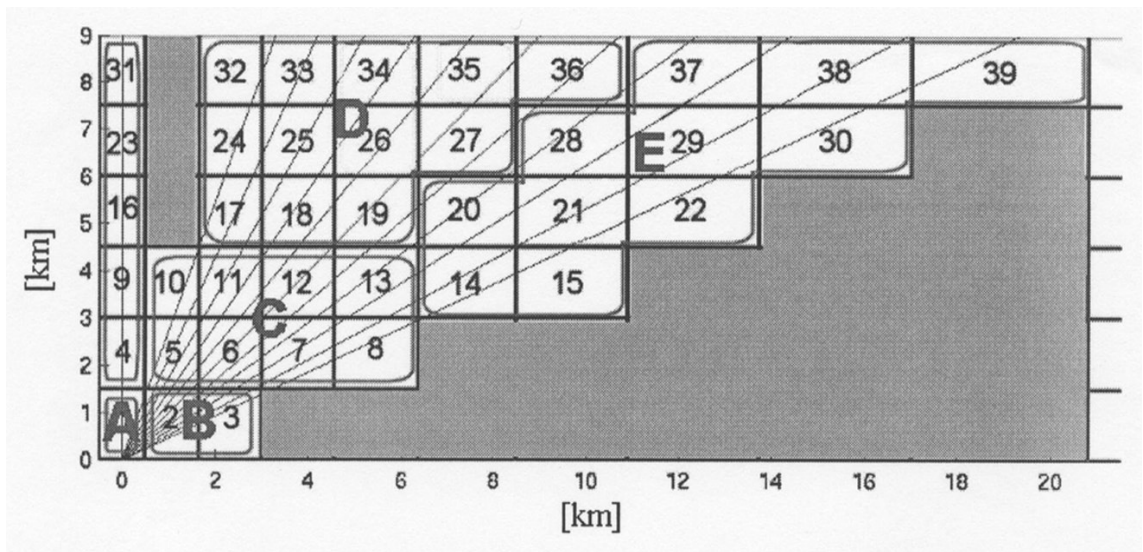
Figure 2.2 The scanned vertical plane is divided into resolution bins, identified by numbers, each with constant attenuation. The maximum altitude and maximum range are fixed at 9 km and 23 km, respectively, determined by the assumed maximum height of water vapor and the elevation of the lowest scan. Solid lines represent the propagation paths "observed" by the radiometer antenna. Since the problem is ill-conditioned, a re-parameterization allowed the 39 bins to be re-expressed into five macrocells, identified by letters, according to the eigenstructure of the Jacobian matrix [18].

2.4 3-D Water Vapor Field using a Network of Radiometers

Three-dimensional water vapor density is retrieved from brightness temperatures measured by a network of microwave radiometers, such as CMR-H, using algebraic reconstruction tomography, optimal estimation and Kalman filtering [6]. In a demonstration network, three radiometers are stationed in a triangular topology to. This process is briefly summarized as follows. The vertical plane scanned by the radiometer is divided into grid cells, as shown in conceptual form in Figure 2.3. The set of elevation angles with minimum redundancy is determined by calculating the number of non-zero eigenvalues of the Jacobian matrix [6] relating the variation of brightness temperatures and absorption coefficients. Brightness temperatures are measured at each of the elevation angles. The number of eigenvalues is equal to the total number of independent

24

ray intersections inside of unique grid cells. Figure 2.4 shows the number of eigenvalues as a function of the number of elevation angles measured by an elevation-angle scanning radiometer. A water vapor profile from radiosonde(s) is used as an *a-priori* or reference profile. Assuming the reference atmospheric state, a radiative transfer equation in discrete form is used to calculate the brightness temperature at each measurement frequency that would be measured by a radiometer pointing at each elevation angle. The difference between the measured and calculated brightness temperatures is termed the variation in brightness temperature. The absorption coefficient in each of the grid cells is calculated using state-of-the-art absorption models [20] [21] [22]. The variation of the brightness temperature at each elevation angle and the variation of the absorption coefficient in each grid cell are related by the elements of the Jacobian matrix. Calculating the absorption coefficient from the brightness temperature variation and the Jacobian matrix is an ill-posed problem because the number of measurements is less than the number of grid cells at which the absorption coefficient needs to be known. For that reason, the deviation of each absorption coefficient from its reference value is calculated using Bayesian optimal estimation. The absorption coefficient retrieved in this way for each of the four brightness temperature measurement frequencies is fit to the Van-Vleck Weisskopf model [23] of the water vapor absorption line to retrieve the water vapor density in each of the grid

cells. In addition, spatial interpolation (kriging) is used to retrieve the water vapor density

Figure 2.3. The vertical plane scanned by the radiometer is divided into grid cells to perform the 3-D water vapor retrieval.

at each of the unsampled locations. The 3-D water vapor can be retrieved with a vertical

spatial resolution of 0.5 km and a similar horizontal spatial resolution [6]. The temporal

resolution of the retrieved water vapor field is dependent on the time required to scan the

spatial volume measured by the three radiometers. In the case of the METAWAVE

experiment, the 3-D water vapor field can be retrieved with a temporal resolution of

approximately 10 minutes. An observation system simulation experiment performed

using Weather Research and Forecasting (WRF) model data showed that the water vapor

density expected percent error was approximately 15-20% [6].
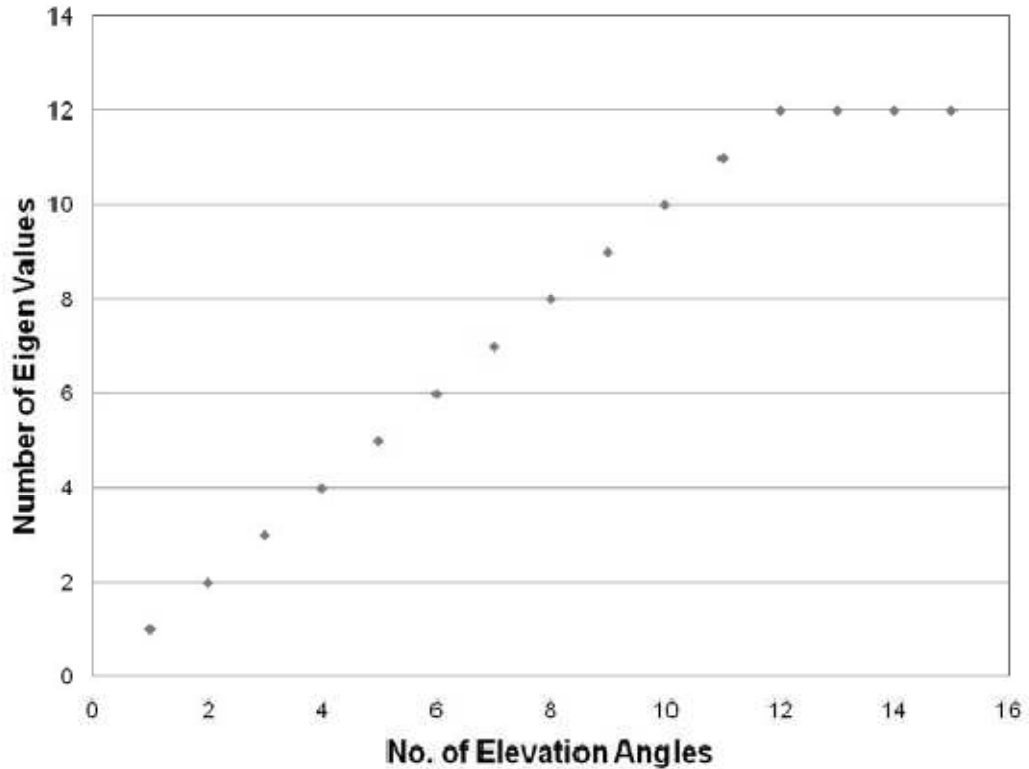
Figure 2.4. The number of eigenvalues of the Jacobian matrix vs. the number of elevation angles of a scanning microwave radiometer [6].

2.5 Potential for Assimilation of the High Resolution Water Vapor Density Profiles into Numerical Weather Prediction Models

As already discussed, high resolution water vapor and temperature profiles can be very useful in numerical weather prediction (NWP). There are several methods by which observations from various remote sensing instruments can be assimilated into NWP models [24]:

1. Brightness temperature measurements, their error estimates and radiometric sensitivity as well as any constraints due to the underlying relationships due to physics can be provided as inputs into the NWP. This could be done by providing data from different

27

instruments operated at the same site i.e., geographically collocated instruments or from different instruments located at different sites.

2. Profiles of atmospheric parameters (with error estimates) retrieved using the variational method can be fed continuously into the NWP as input. The profiles could be retrieved either from:

a. A 1-D variational retrieval technique combining observations from different instruments with *a-priori* from radiosondes or NWP forecasts. These retrieved profiles of parameters could then be assimilated directly into a 3-D or 4-D variational retrieval method for NWP.

b. Provide a continuous data stream of atmospheric profiles (with error estimates) retrieved using various retrieval techniques like neural networks or another regression technique. It would also be useful to provide real-time data on the high-resolution 3-D water vapor field. This would allow the retrieval of small changes in the profiles like water vapor and temperature, which could be lost if assimilated into an NWP model with coarser vertical resolution. This approach would also be useful for nowcasting applications.

Chapter 3

3-D Water Vapor Retrievals as part of the Mitigation of Electromagnetic Transmission Errors induced by Atmospheric Water Vapor Effects (METAWAVE) experiment

3.1 INTRODUCTION

As discussed in section 2.1 high resolution water vapor data can be used for initialization of numerical weather prediction models. Similarly the 3-D water vapor field can be used to mitigate the effect of errors introduced due to water vapor on the digital elevation maps of Spaceborne Interferometric Synthetic Aperture Radar (InSAR). InSAR imaging has been used for over a decade to monitor tectonic movements and landslides on the cm scale. Since tectonic movements have to be observed on a scale of centimeters InSAR data has to be very accurate. InSAR makes use of the difference in phase information between two synthetic aperture radar (SAR) images taken at different times or from different viewing angles, resulting in an interferogram [25]. The interferograms can be affected by the spatial and temporal variability of water vapor. The spatial and temporal variability of water vapor, pressure and temperature introduce changes in the round-trip propagation delay of the signals transmitted and received by the radar. The effect of water vapor variability can be reduced by averaging a large number of interferograms [26], just as the effect of uncorrelated noise decreases when averaging large number of independent samples. It can also be estimated by analyzing a long sequence of interferometric phase of very stable and coherent permanent scatterers, i.e.,

the PS technique [27]. However, intervening sudden surface deformation prevents such averaging and multi-image approaches. In these cases, the availability of high-resolution spatial and temporal information on atmospheric water vapor would be useful to mitigate its effect on interferograms. Therefore a field experiment was performed by European Space Agency (ESA) to look at various methods of retrieving water vapor density fields. This chapter focuses on measurements performed during the Mitigation of Electromagnetic Transmission errors induced by Atmospheric Water Vapor Effects (METAWAVE) experiment sponsored by the ESA. As part of METAWAVE, the Microwave Systems Laboratory at Colorado State University deployed a network of Compact Microwave Radiometers for Humidity profiling to measure the 3-D water vapor density over Rome, Italy.

This chapter discusses the METAWAVE experiment and presents the results of the 3-D water vapor retrieval. A comparison is presented between measurements from the network of Compact Microwave Radiometers for Humidity profiling and those from other spaceborne instruments and results from a numerical weather prediction model. In Section 3.1 the background of the METAWAVE experiment is discussed. Section 3.2 describes the experimental setup for the field experiment, the Compact Microwave Radiometer for Humidity profiling, the Moderate Resolution Imaging Spectroradiometer (MODIS) and the Medium Resolution Imaging Spectrometer (MERIS). Section 3.3 summarizes the 3-D water vapor retrieval technique. Section 3.4 discusses the results of the experiment, focusing on the 3-D water vapor field retrieved from the radiometer network and on the comparison of the integrated water vapor field from CMR-H network with measurements from the Moderate Resolution Imaging

Spectroradiometer (MODIS) on NASA's Aqua satellite, as well as those from the Medium Resolution Imaging Spectrometer (MERIS) instrument onboard ESA's Environmental Satellite (ENVISAT). Conclusions are presented in Section 3.5.

3.2. EXPERIMENT DESCRIPTION

As part of the METAWAVE experiment, the Microwave Systems Laboratory at Colorado State University (CSU) deployed in Rome, Italy, a ground-based network of scanning Compact Microwave Radiometers for Humidity profiling (CMR-H) [5] that were custom-built at CSU to observe 3-D water vapor density with fine spatial and temporal resolution. Three CMR-Hs were deployed in a triangular topology to implement a three-node network of scanning radiometers, as shown in Figure 3.1.
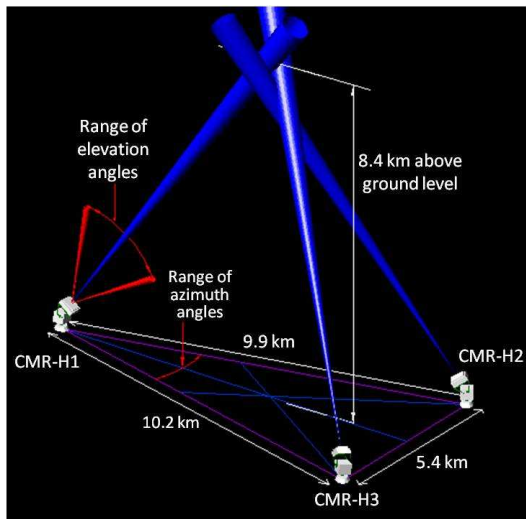
Figure 3.1. Schematic depiction of three Compact Microwave Radiometers for Humidity profiling scanning the atmosphere over Rome, Italy, in azimuth and elevation angles. Each radiometer scanned elevation angles from 30^0 to 80^0 at three different azimuth angles, i.e. along the two baselines connecting it with the other two radiometers and along the median of those baselines.

The three radiometers were located at Sapienza University of Rome (Engineering Faculty) and Tor Vergata University of Rome, as well as a third location, Picco Tre

Signori. Table 3.1 gives the latitude and longitude of the location of the radiometers in Rome. The three radiometers scanned the atmosphere above the triangular network in azimuth and elevation angles, as shown in Figure 3.1.

Radiometer	Site	Latitude	Longitude
CMR-H1	Tor Vergata	41.850 ^{0}N	12.598 ^{0}E
CMR-H2	Sapienza (via Eudossiana)	41.894 ^{0}N	12.494 ^{0}E
CMR-H3	Picco Tre Signori	41.930 ^{0}N	12.537 ^{0}E

Table 3.1. Locations of ground-based Compact Microwave Radiometer Network deployed in Rome, Italy

A scanning strategy was chosen for maximal coverage of the atmosphere above the network with a repeat period of 10 minutes. Each radiometer viewed three azimuth angles and 10 angles in elevation from 10º zenith angle to 30º above the horizon, i.e. elevation angles of 30º to 80º. The three azimuth angles scanned by each radiometer are represented by yellow segments on the map in Figure 3.2.
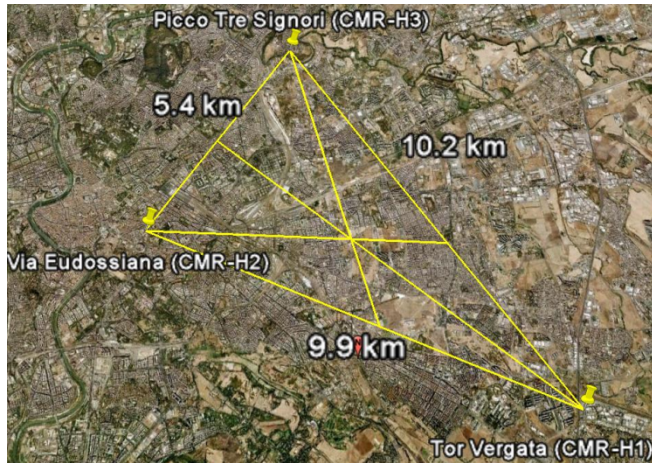
Figure 3.2. Map showing the locations of the three nodes of the network of Compact Microwave Radiometers for Humidity profiling deployed in Rome, Italy, during the METAWAVE experiment in September and October 2008.

Figure 3.3. Deployment of CMR-H on the terrace of Sapienza University of Rome for the METAWAVE experiment.

These ground-based measurements were performed from 20-Sept-2008 to 03-Oct-2008, a period that included a number of overpasses of MODIS on NASA's Aqua satellite and of MERIS and the Advanced Synthetic Aperture Radar (ASAR) on ESA's ENVISAT. A photograph of the deployment of a CMR-H, on the terrace of Sapienza University of Rome, is shown in Figure 3.3.

3.2.1. **Compact Microwave Radiometer for Humidity Profiling**

Developed using state-of-the-art monolithic microwave integrated circuit (MMIC) technology, the Compact Microwave Radiometer for Humidity profiling (CMR-H) is a low-mass, low-power and small-volume microwave radiometer that measures simultaneously at four optimally-selected K-band frequencies near the 22.235 GHz water vapor absorption line, i.e. 22.12, 22.67, 23.25 and 24.5 GHz. Table 3.2 shows the specifications of the CMR-H.

Mass (kg)	Dimensions (cm)	Power (W)	Beamwidth (deg)	Temp. Stability (°C)
6	24 x 18 x 16	50	3-4	0.1

Table 3.2. Specifications of the Compact Microwave Radiometer for Humidity profiling (CMR-H)

The radiometer has a radiometric resolution (NEΔT) of 0.2 K for an integration time of 3 seconds [5]. The CMR-H has been deployed and tested during previous experiments, in which its ability to retrieve atmospheric water vapor has been demonstrated [6]. In this paper, a network of CMR-Hs is implemented in order to demonstrate its capability to retrieve water vapor with quality comparable to that of well-known water vapor observations, including the MODIS and MERIS integrated water vapor products.

3.2.2 Moderate Resolution Imaging Spectroradiometer

The MODIS instrument has 36 channels spanning the spectral region between 0.4 and 15 µm. Five channels in the near-infrared region of 0.8–1.3 µm are used for remote sensing of water vapor. Water vapor absorption channels with decreasing absorption coefficients are centered at 0.936, 0.940, and 0.905 µm, respectively. The strong absorption channel at 0.936 µm is most useful under dry conditions, while the weak absorption channel at 0.905 µm is most useful under very humid conditions, or low solar elevation angles [28]. The retrieval technique relies on comparing the magnitude of solar radiation reflected from the ground at absorbing and non-absorbing channels in order to detect its absorption by water vapor from the surface to the sensor. The equivalent total vertical amount of water vapor is retrieved from a comparison between the reflected solar radiation in the absorbing channel with that in nearby non-absorbing channels. MODIS has spatial resolution of 1 km, but operational IWV are available at 5-km resolution [28].

3.2.3 Medium Resolution Imaging Spectrometer

MERIS's main objectives are to observe ocean color to understand the ocean carbon cycle, to estimate cloud type and albedo, top and bottom of atmosphere vegetation indices and other geophysical parameters [29]. MERIS retrieves total columnar atmospheric water vapor over the entire Earth once every 3 days. MERIS has 15 programmable spectral frequency bands, two of them in the near-infrared and referred to as the water vapor channels, i.e. the absorption-free band at 885 nm and the absorption band at 900 nm. MERIS retrieves the total water vapor column based on differential absorption between these two nearby water vapor bands. MERIS near-infrared water vapor products are available at full resolution of 300 m and at reduced resolution of 1200 m[29]. Finer spatial resolution than previous polar orbiting instruments makes MERIS very useful to the meteorological community for observing integrated water vapor on a global basis with a spatial resolution of hundreds of m. The MERIS product with full resolution was used for comparison with data from the CMR-H network.

3.3 RETRIEVAL OF THREE-DIMENSIONAL WATER VAPOR DENSITY

Three-dimensional water vapor density is retrieved from the brightness temperatures measured by the CMR-H network using algebraic reconstruction tomography, optimal estimation and Kalman filtering [6]. This process is briefly summarized here. The vertical plane scanned by the radiometer is divided into grid cells, as shown in Figure 3.4. A water vapor profile from radiosonde(s) is used as an *a-priori* or reference profile. Assuming the reference atmospheric state, a radiative transfer equation in discrete form is used to calculate the brightness temperature at each measurement

frequency that would be measured by a radiometer pointing at each elevation angle. The difference between the measured and calculated brightness temperatures is termed the variation in brightness temperature. The absorption coefficient in each of the grid cells is calculated using state-of-the-art absorption models [20] [21] [22]. The variation of the brightness temperature at each elevation angle and the variation of the absorption coefficient in each grid cell are related by the elements of the Jacobian matrix. Calculating the absorption coefficient from the brightness temperature variation and the Jacobian matrix is an ill-posed problem because the number of measurements is less than the number of grid cells at which the absorption coefficient needs to be known. For that reason, the deviation of each absorption coefficient from its reference value is calculated using Bayesian optimal estimation. The absorption coefficient retrieved in this way for each of the four brightness temperature measurement frequencies is fit to the Van-Vleck Weisskopf model [23] of the water vapor absorption line to retrieve the water vapor density in each of the grid cells. In addition, spatial interpolation (kriging) is used to retrieve the water vapor density in each of the unsampled locations. The 3-D water vapor can be retrieved with a vertical spatial resolution of 0.5 km and with a similar horizontal spatial resolution [6]. The temporal resolution of the retrieved water vapor field is dependent on the time required to scan the spatial volume measured by the three radiometers. In the case of the METAWAVE experiment, the 3-D water vapor field can be retrieved with a temporal resolution of approximately 10 minutes.
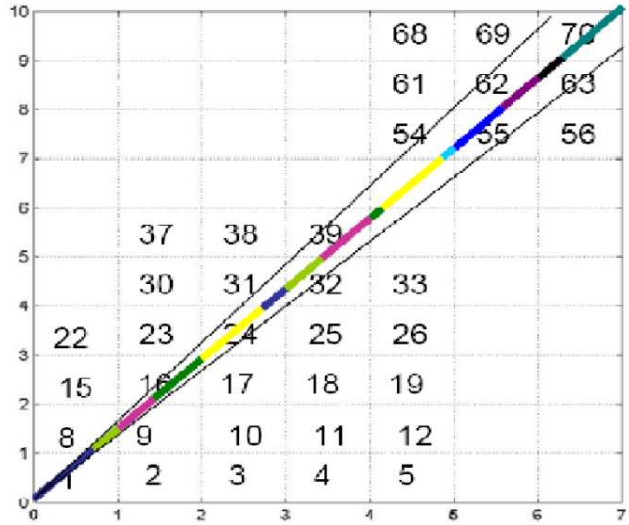
Figure 3.4. The vertical plane scanned by the radiometer is divided into grid cells to perform the 3-D water vapor retrieval.

3.4. RESULTS OF THE EXPERIMENT

Radiometric measurements were performed at the four frequencies of 22.12, 22.67, 23.25 and 24.5 GHz. The brightness temperatures were used to retrieve the 3-D water vapor field over the area scanned by the radiometers. Here in section 3.4.1 the brightness temperatures from CMR-H are compared with the brightness temperature from radiosonde and dual channel radiometer from Radiometrics. In section 3.4.2 the 3-D water vapor from CMR-H network has been presented while a discussion of the comparison of 2-D water vapor from CMR-H network and the MM5 model is presented in section 3.4.3. The comparison between CMR-H and MODIS and MERIS is presented in section 3.4.4 and 3.4.5 respectively.

3.4.1 3-D WATER VAPOR DENSITY RESULTS

The 3-D water vapor density field was retrieved from the brightness temperature measurements by the three CMR-Hs during the METAWAVE experiment Horizontal slices of the retrieved water vapor density at altitudes of 0.5 km, 2.0 km and 3.0 km above ground level at 21:30 UTC on 20-Sept-2008, near the overpass time of the ASAR on ENVISAT, are shown in Figure 3.10. The size of each pixel in this figure is 500 x 500 m. The water vapor profile from a radiosonde launched at 21:30 UTC on 20-Sept-2008 was used as the *a-priori* for retrieving the 3-D water vapor field. The variability of water vapor densities in each horizontal slice is approximately 23.8%, 17.0% and 5.0% at 0.5 km, 2.0 km and 3.0 km altitudes, respectively. This shows that atmospheric water vapor densities with large dynamic range have been retrieved, demonstrating the ability of the CMR-H network to sense substantial variability in water vapor density and that it compares fairly well with numerical simulations.
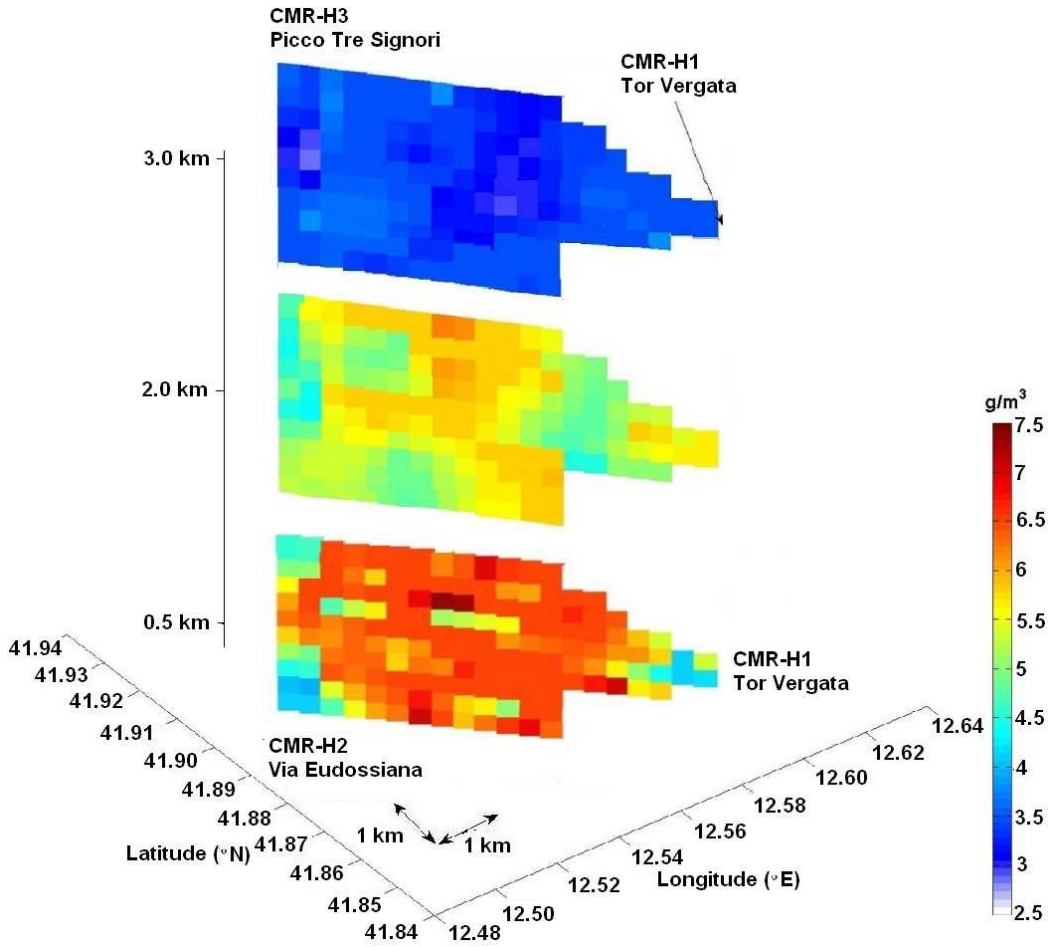
Figure 3.5. Water vapor density from CMR-H observations at three altitudes above ground level. The vertical axis is not to scale.

3.4.2 Comparison of 2-D Water Vapor Results from CMR-H and MM5 Model Output

The 2-D water vapor output from the Mesoscale Model 5 (MM5) was compared to 2-D water vapor densities retrieved from the CMR-H network. The MM5 numerical

weather prediction model has a horizontal resolution of 1 km on the inner domain and a variable vertical resolution [30]. Figures 3.11(a) and 3.11(b) show comparisons of the 2-D water vapor from the MM5 model and from the CMR-H network for 20-Sept-2008 at 21:40 UTC and 03-Oct-2008 at 10:10 UTC, respectively. The measurement time interval or temporal resolution of the radiometer retrievals is 10 minutes. In the lowest 2 km of the troposphere, the CMR-H network retrievals show greater water vapor density and more variability than the MM5 model output on both days. At altitudes of 3 km and higher in Figure 3.11(a), the water vapor densities for both CMR-H network retrievals and MM5 model output range from 1 to 4 g/m^3. Again at altitudes of 3 km and higher, Figure 3.11(b) shows values for CMR-H network retrievals ranging from 2 to 5 g/m^3, and MM5 model outputs range from 2 to 4.5 g/m^3. Thus the water vapor density in the middle and upper troposphere is nearly the same for CMR-H network retrievals and MM5 model output for these cases. As shown in Figure 3.11(a), the MM5 model output has a maximum water vapor density of approximately 8 g/m^3, while the CMR-H network retrievals have a maximum value of approximately 9.5 g/m^3. Figure 3.11(b) shows larger values of water vapor density on 03-Oct-2008 than those of Figure 3.11(a) on 20-Sept-2008. From these results, we conclude that the CMR-H network retrievals exhibit similar spatial variability and average values to those of the MM5 numerical weather model output.
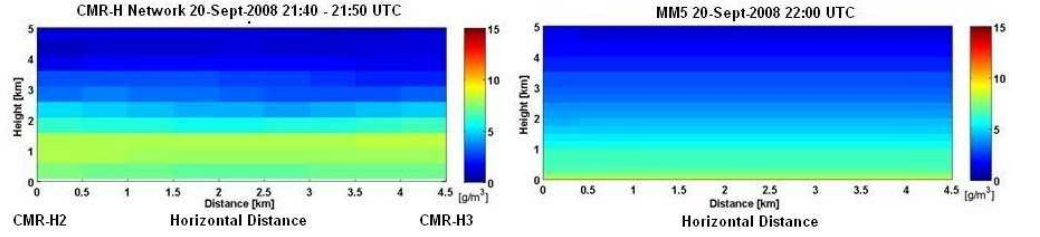
(a)
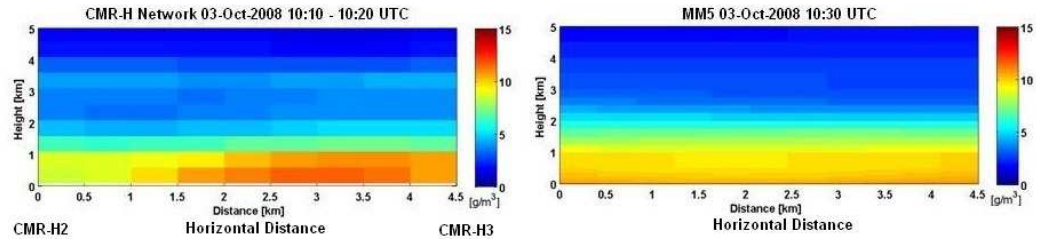
(b)

Figure 3.6. Comparison between the 2-D water vapor retrieved from the CMR-H network and MM5 model results (a) on 20-Sept-2008 and (b) on 03-Oct-2008.

3.4.3 Comparison of Integrated Precipitable Water Vapor from CMR-H Network and MODIS

A comparison of the vertically integrated precipitable water vapor (IWV) retrieved from the CMR-H network and the MODIS instrument on NASA's Aqua satellite is presented here. The 3-D atmospheric water vapor densities retrieved from the CMR-H network have been vertically integrated to obtain IWV at each horizontal lat/lon location. Then these IWV results have been decimated to a spatial resolution of 1 km in order to compare them with the IWV from MODIS. From Figure 3.12, it is observed that the CMR-H and MODIS IWV retrievals have similar values. This analysis was

performed to compare the average IWV of the CMR-H network retrievals with the average IWV of the MODIS retrievals.
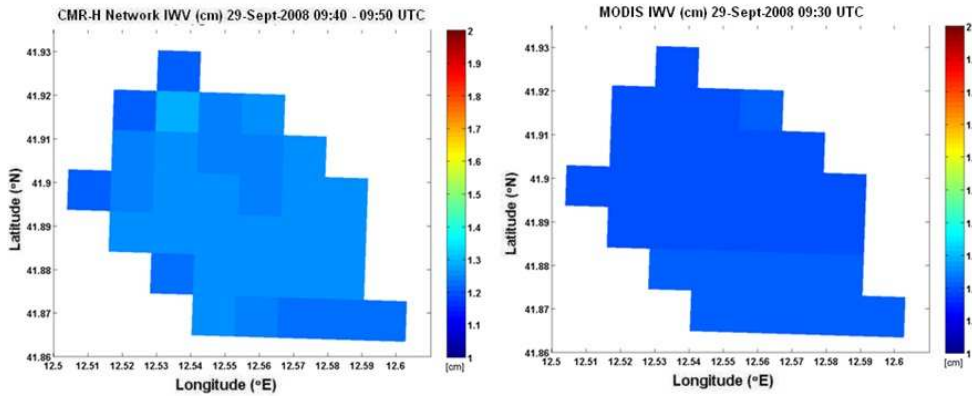
Figure 3.7. Comparison between integrated precipitable water vapor from the CMR-H network and MODIS on 29-Sept-2008.

In Figure 3.12, the average IWV from MODIS is 1.23 cm while the average of the CMR-H network retrievals is 1.28 cm. It should be noted that the MODIS water vapor products have an accuracy of 5-10% [22]. Since the average value of IWV retrieved from the CMR-H network and from MODIS agree to within the accuracy of MODIS water vapor retrievals, we conclude that the CMR-H network retrievals yield a good average value of IWV.

3.4.4 COMPARISON OF INTEGRATED PRECIPITABLE WATER VAPOR FROM CMR-H NETWORK AND MERIS

A comparison of the IWV values retrieved from MERIS on ESA's ENVISAT and the CMR-H network is presented here. Spatially and temporally coincident MERIS IWV and CMR-H network IWV were used for the comparison. Comparisons of the IWV from the CMR-H network retrievals with the MERIS retrievals for 29-Sept-2008 at 09:50 UTC and 30-Sept-2008 at 09:20 UTC are shown in Figures 3.13 and 3.15, respectively.

The *a-priori* for the CMR-H network retrieval shown in Figure 3.13 is an average of water vapor profiles from radiosondes launched at 6:00 UTC and 12:00 UTC on 29-Sept-2008 from Pratica di Mare, a station located about 25 km southwest of the center of the CMR-H network in Rome. The CMR-H IWV data has a horizontal resolution of 500 m. Since the full-resolution products of MERIS have been used, the CMR-H network retrievals have been interpolated to produce water vapor images with 300-m spatial resolution. There are 394 pairs of co-located spatial samples from MERIS and CMR-H network on 29-Sept-2008 from 09:40 UTC – 09:50 UTC. The average IWV value of the CMR-H network retrievals is 1.29 cm, while the average IWV of the MERIS retrievals is 1.30 cm.
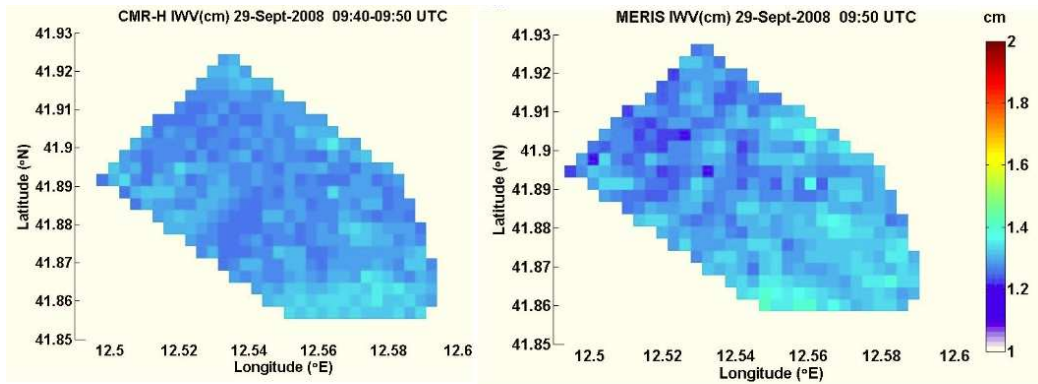
Figure 3.8. Comparison between integrated precipitable water vapor from the CMR-H network and MERIS on 29-Sept-2008.
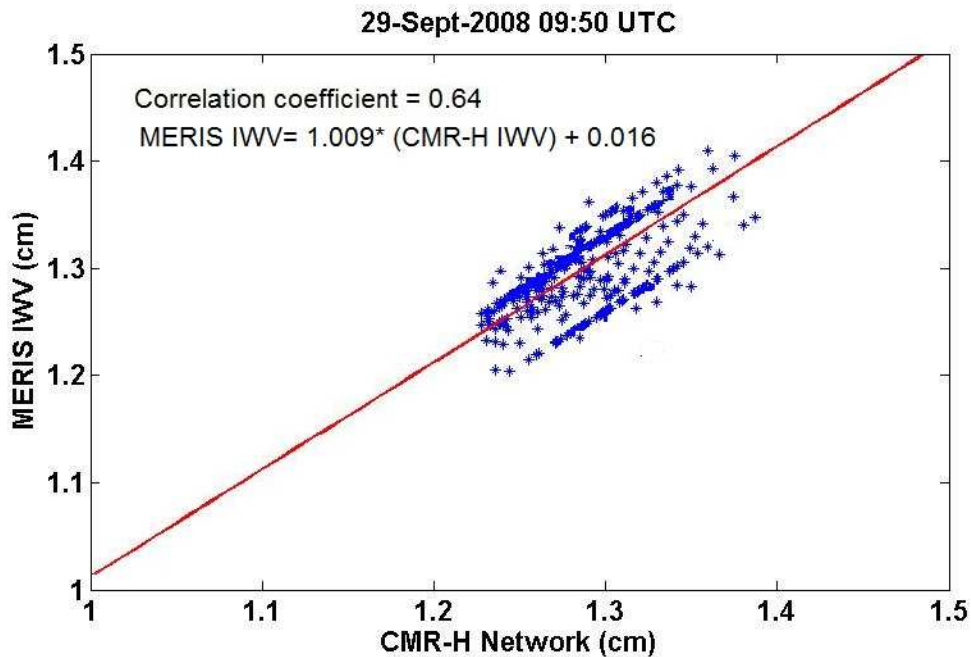
Figure 3.9. Scatter plot for MERIS and CMR-H integrated precipitable water vapor on 29-Sept-2008.

Figure 3.14 shows the correlation between the IWV from MERIS retrievals and those from the CMR-H network retrievals. The solid line represents the best fit between the two sets of data. The correlation coefficient is 0.64. A linear fit yielded the relationship MERIS IWV= 1.009*(CMR-H IWV) + 0.016 cm. The mean of the difference between

the two data sets (i.e., bias) is 0.01 cm. The standard deviations of the MERIS and CMR-H network retrievals are 0.023 cm and 0.034 cm, respectively. The absolute value of the difference in IWV between the MERIS and CMR-H network retrievals is approximately 0.1 to 0.6 mm.

A similar comparison was performed for 30-Sept-2008 from 09:15 – 09:25 UTC, as shown in Figure 3.15. As in the previous case, the *a-priori* for the CMR-H network is an average of water vapor profiles from radiosondes launched from Pratica di Mare at 6:00 UTC and 12:00 UTC on 30-Sept-2008. Again, there are 394 pairs of co-located spatial samples from MERIS and CMR-H network. The correlation between the IWV from MERIS retrievals and that from the CMR-H network retrievals is shown in Figure 3.16. In contrast to Figure 3.15, the IWV data are scattered widely on both sides of the linear fit, whereas in Figure 3.15 the data are close to the best fit line. Correspondingly, a somewhat lower correlation coefficient of 0.51 is observed. A linear fit yielded the relationship MERIS PWV =0.975*(CMR-H IWV) - 0.032 cm. The mean of the difference between the MERIS and CMR-H network data is -0.0151 cm. The standard deviations of the IWV data from MERIS and CMR-H network retrievals are 0.034 cm and 0.028 cm, respectively. The absolute value of the difference in IWV between the MERIS and CMR-H network retrievals is approximately 0.2 to 0.75 mm.
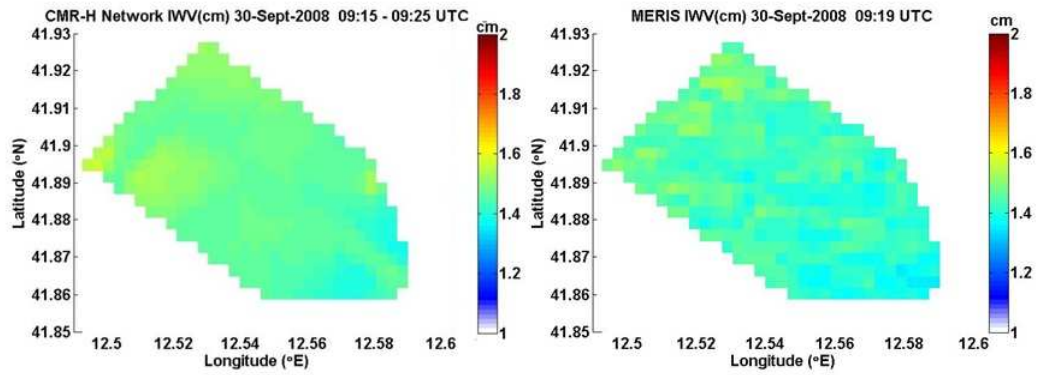
Figure 3.10. Comparison of integrated precipitable water vapor from the CMR-H network and MERIS on 30-Sept-2008
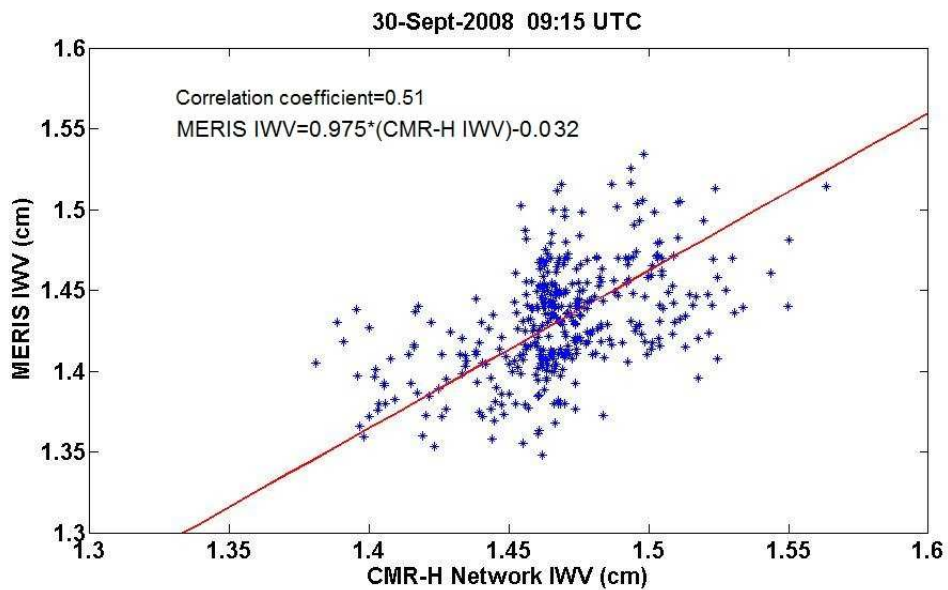
Figure 3.11. Scatter plot for MERIS and CMR-H integrated precipitable water vapor on 30-Sept-2008.

The mean values and ranges of the differences between the two IWV data sets show quite good agreement in moderately humid conditions. The absolute value of the difference between the MERIS and CMR-H network data in both of the two cases considered is between 0.1 to 0.75 mm, while the error of water vapor content for MERIS over land is 1.65 mm rms [31]. Since the differences between the IWV from MERIS and CMR-H network retrievals are significantly smaller than the error of MERIS retrievals, the CMR-H network retrievals compare very well with MERIS retrievals. Therefore, in comparison to satellite data sources, the CMR-H network retrievals have good potential to correct for variations in wet-tropospheric delay in InSAR imagery.

3.5. CONCLUSION

Results from brightness temperature measurements from a ground-based Compact Microwave Radiometer for Humidity profiling Network during the METAWAVE experiment demonstrate the ability to retrieve 3-D water vapor with high accuracy. The retrieval technique achieves a vertical and horizontal resolution of 500 meters and a time resolution of approximately 10 minutes. These retrievals use water vapor profile from nearby radiosondes as the *a-priori*. Comparisons between retrievals from CMR-H network-measured brightness temperatures and passive optical measurements from the MODIS and MERIS instruments aboard polar-orbiting satellite instruments show that CMR-H network retrievals of 3-D water vapor show good potential to correct InSAR imagery for variations in wet-tropospheric delay. Additionally, in contrast to the poor temporal coverage of polar-orbiting satellites, CMR-H networks have the potential to provide water vapor data continuously with 500-m spatial and 10-minute temporal resolution for all of the locations where they are deployed.

A good method to compare and validate the available CMR-H network and MERIS data would be to correct an interferogram retrieved from ENVISAT's ASAR using the CMR-H network 3-D water vapor density retrievals as well as the MERIS IWV retrievals and then to compare the two corrected maps. Such an interferogram should use the phase difference between two SAR images measured at different times. However, the two overpasses of the ASAR during the period of the METAWAVE experiment were during different orbits, one of which was ascending and the other of which was descending. Therefore, ASAR interferograms could not be obtained for the dates and times of the METAWAVE experiment, and no ASAR interferograms could be corrected using the CMR-H network retrievals. From the comparison of the CMR-H network data with the MERIS data it has become clear that MERIS and CMR-H network retrievals agree well under moderately humid conditions and can be used to retrieve columnar water vapor content with a difference of 0.1 to 0.75 mm for geographically co-located pixels. These results demonstrate the capability of the CMR-H network to retrieve IWV with high spatial and temporal resolution, while maintaining quality comparable to that of mature water vapor products. More comparisons need to be performed in order to validate the 3-D water vapor density retrievals from CMR-H network brightness temperature measurements and to determine definitively whether or not such retrievals can be used to correct InSAR images for variations in wet-tropospheric path delay. The exploitation of a long time sequence of SAR acquisitions over Rome, Italy using the PS technique [27]will potentially provide path delay estimates that could be compared to the CMR-H products.

Chapter 4

Enhancement of Vertical Resolution of 1-D Water Vapor Profile Retrieval

4.1 Introduction

Thermodynamic properties of the troposphere, particularly water vapor content and temperature, change in response to physical mechanisms, including frictional drag, evaporation, transpiration, heat transfer, pollutant emission and flow modification due to terrain. The planetary boundary layer (PBL) is characterized by a greater rate of change in its thermodynamic state than higher tropospheric altitudes. Such changes in the PBL typically occur on time scales of less than one hour; whereas the upper troposphere exhibits much longer time constants. Large horizontal gradients in vertical wind speed and steep vertical gradients in water vapor and temperature in the PBL result in high-impact weather, including severe thunderstorms. Observation of these gradients in the PBL with improved vertical resolution is important for improvement of weather prediction. Additionally high vertical resolution and accuracy of measured thermodynamic profiles, especially water vapor and temperature, are important for initialization of numerical weather prediction models. Therefore the objective of this study is to determine the water vapor profile with high vertical resolution and also the planetary boundary layer height. There are various methods to determine the PBL height,

like using gradient of water vapor, temperature and wind movement. Usually the boundary layer has a height varying from 500 meters to 3000 meters depending on the time of day and the time of year. During the day and in warm seasons the boundary layer height tends to be higher than during the night and in cold seasons. The top of the PBL is typically characterized by an inversion in the temperature and water vapor density profile. In meteorology, an inversion is a deviation from the normal rate of change of atmospheric thermodynamic property (like water vapor and temperature) with altitude [32]. Water vapor density and temperature usually decrease with altitude. But when there is an inversion, values of water vapor density and temperature start increasing instead of decreasing.

Therefore to determine the height of the PBL, water vapor density needs to be measured with a very high vertical resolution of a few hundred of meters or so. Radiosondes measure water vapor density profiles with a vertical resolution of approximately 10 meters in the lower troposphere. But the use of radiosondes is typically limited to twice per day. Satellite remote sensing in the visible, infrared and microwave bands provides qualitative and quantitative measurements of many atmospheric properties, including cloud cover, precipitation, liquid water content and precipitable water vapor in the atmosphere above the PBL. However, its ability to characterize thermodynamic properties of the PBL is limited by the confounding factors of ground emission in microwave channels and of cloud cover in visible and IR channels, as well as limitations in the vertical and temporal resolution of the remote sensing instruments onboard the satellite. As already discussed, the PBL changes a lot within a time period of around 1 hour. So there is a requirement to keep track of changes in the thermodynamic

state of the atmosphere with a high temporal resolution. This can be done by using passive remote sensing instruments like microwave radiometers. Typically microwave radiometers have a coarse resolution of hundreds of meters or more. Therefore the resolution of water vapor density and temperature profiles retrieved from radiometric measurements need to improved. The better we can distinguish the variation in these parameter with small increment in altitude the better the resolution.

Here a new technique has been used to improve the vertical resolution of retrieved water vapor density profiles, based on the design of the Compact Microwave Radiometer for Humidity Profiling (CMR-H). Here the vertical resolution has been enhanced by using the Backus-Gilbert technique. Backus and Gilbert technique has been used since 1968 for deriving geophysically useful inferences about the internal structure of the Earth from a limited number of measurements of gross Earth data, like seismic travel times between various sources and observers. This technique has been used in atmospheric remote sensing since 1972 when it was introduced in the remote sensing world [33] to increase the vertical resolution of the temperature profiles obtained from measurements of brightness temperature.

State-of-art techniques used to get a good vertical resolution from a given data set, increase the sensitivity of the retrieved profiles to random noise [33]. Therefore a tradeoff exists between resolution and its stability to variation in noise . This can be taken care of by the Backus-Gilbert technique by minimizing a linear combination of vertical resolution and noise. Thus the vertical resolution is enhanced, while estimating the sensitivity of resolution to noise. This technique has been used in passive remote sensing as well as active remote sensing like Radio Detection And Ranging [34].

This technique is described in subsequent sections.

4.2 Backus-Gilbert Theory

In atmospheric remote sensing, a water vapor profile is retrieved by the inversion of radiometer brightness temperature measurements near a water vapor absorption line. The set of brightness temperature measurements T_{Bi} is related to the actual water vapor profile by the forward model, given by

$$T_{Bi} = \int K_i(z')x(z')dz' + \varepsilon$$

(4.1)

where i is an index for the number of measurements and is given by i $=1,\ldots..$m, T_B is the measurement or brightness temperature and x(z') is profile to be retrieved.

K is the kernel function while ε is the measurement error due to instrument noise. A kernel function for an atmospheric parameter (such as water vapor or temperature) is the change in the measured brightness temperature due to a unit change in that parameter, e.g. water vapor density, at a particular altitude in a 1-km thick layer. Therefore, a kernel function is the sensitivity of measured T_B to changes in that parameter, e.g. water vapor, at a particular altitude.

The kernel function is given as

$$W_{\rho v}(f,\theta,z) = K_{\rho v}(f,\theta,z) = \frac{\partial \kappa_a(z)}{\partial \rho_v(z)}[T(z) - T_B(f,\theta,z)]e^{-\tau(0,z;\theta;f)\sec(\theta)}\sec(\theta)$$

(4.2)

where

- $\kappa_a(z)$ is the absorption coefficient of the atmosphere at a height z,
- $\rho_v(z)$ is the water vapor density at height z,
- T(z) is the temperature at altitude z,

- T_B is the brightness temperature at frequency f and elevation angle θ, and
- τ is the opacity.

The estimate of profile $\hat{x}(z)$ is given by the following

$$\hat{x}(z) = \sum_{i=1}^{m} G_i(z) T_{Bi} \tag{4.3}$$

where G(z) is the coefficients used for estimating water vapor profile.

Substituting equation 4.1 for T_{Bi} in equation 4.3,

$$\hat{x}(z) = \sum_{i=1}^{m} G_i(z) \left[\int K_i(z') x(z') dz' + \varepsilon_i \right] \tag{4.4}$$

$$\hat{x}(z) = \int A(z, z') x(z') dz' + \sum_{i=1}^{m} G_i(z) \varepsilon_i \tag{4.5}$$

where A(z, z') = $\sum_{i=1}^{m} G_i(z) K_i(z')$.

The variability of the width averaging kernel at altitude z determines the resolution of the retrieved profile at level z. It should be noted that a Dirac delta function would be an ideal averaging kernel. If the averaging kernel is a delta function, maximum information is extracted in the form of an estimated profile. But the shape of an averaging kernel is dependent on the shape of the weighting function and also on the number of weighting function available. Since the number of weighting functions that can be used is limited, the averaging kernel would have the shape of a Gaussian distribution which approaches a delta dirac function when the width of the Gaussian distribution is decreased. This Gaussian distribution has some finite spread or width. Spread is the width of the Gaussian distribution at half height. The spread values provide resolution information.

The width of an averaging kernel at a particular altitude is called spread [35]or resolving

length [33]. Spread A (z, z') can also be given by

$$s(z) = \int_{0}^{10km} A^2(z, z')(z' \quad z)^2 dz \qquad (4.6)$$

where $A(z, z')$ is the averaging kernel centered at altitude z.
The figure below shows an illustration of the averaging kernels and their spread.
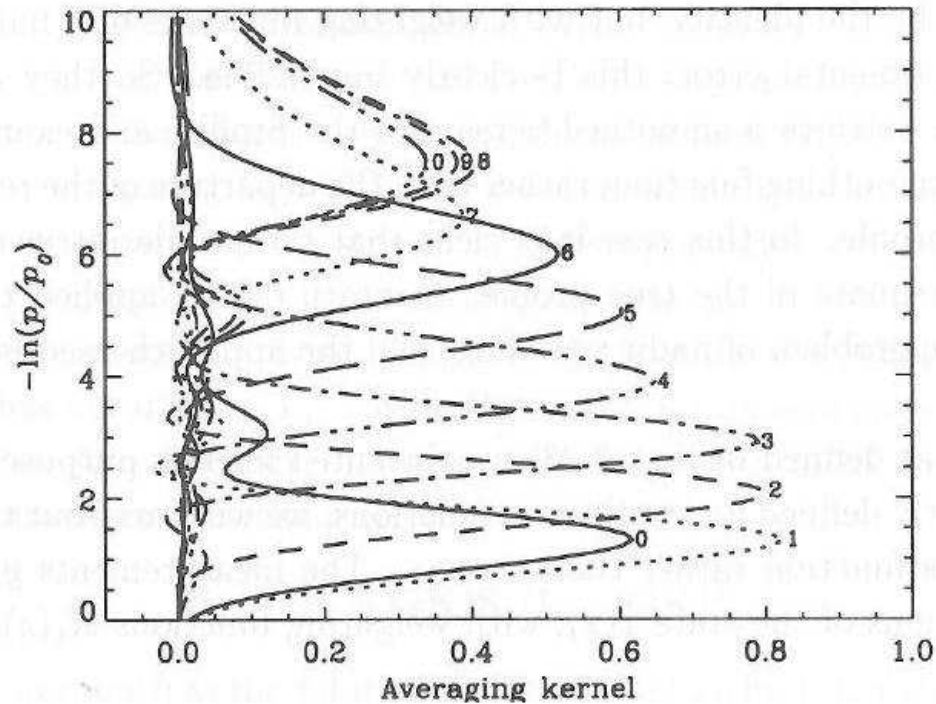
Figure 4.1. Backus-Gilbert averaging kernels with minimum spread [17].

The Figure 4.1 shows the averaging kernels for temperature profile. It shows the various

peaks of solid or dotted or dashed lines. The peaks are centered at different altitudes

which are expressed in terms of pressure. It can be observed that some peaks are

narrower than others. The spread values are directly proportional to width of the peaks. Smaller the spread, higher is the resolution. Here it must be noted that spread values are determined in the vertical direction.

Co-efficients which minimize the spread of averaging kernels can be found subject to the condition that A(z,z') is unimodular. The constraint for the Backus-Gilbert solution is that the averaging kernels should have unit area,

$$\int A(z,z')dz'=1$$

(4.7)

Spread is given by

$$s(z) = 12 \int [\sum_{i=1}^{m} G_i(z)K_i(z')]^2 (z-z')^2 dz'$$

(4.8)

where s(z) can be again written as

$$s(z) = G^T(z)Q(z)G(z)$$

(4.9)

where Q is given by

$$Q_{ij}(z) = 12 \int (z-z')^2 K_i(z') K_j(z')dz'$$

(4.10)

Minimization of the spread with respect to the contribution functions, given the unimodular condition gives the value of the spread as well as the contribution function:

$$\bar{g}(z) = \frac{Q^{-1}(z)\bar{k}}{k^T Q^{-1}(z)\bar{k}}$$

where

$$k = \int K(z)dz$$

(4.11)

$$\bar{g}(z) = \frac{Q^{-1}(z)\bar{k}}{k^T Q^{-1}(z)\bar{k}}$$

substituting g(z) into s(z) gives spread

$$s(z) = \frac{1}{\overline{k}^T Q^{-1}(z)\overline{k}}$$

(4.12)

The spread can be decreased by increasing the number of weighting functions. The weighting functions can be increased by increasing the number of elevation angles at which radiometers scans the atmosphere. The scanning strategy for obtaining the lower spread values is discussed next.

4.3 Scanning Strategy

The vertical resolution depends on the spread of the averaging kernel, which is in turn determined by the number of linearly independent weighting functions used. If the number of weighting functions is increased, the averaging kernel more closely approximates a delta function. This can be accomplished in two ways. One approach is to increase the number of measurement frequencies with high information content, and the second approach is to increase the number of elevation angles of measurements, or a combination of both. Since this study has been conducted based on the CMR-H, the number of measurement frequencies cannot be increased, but the number of elevation angles of measurement can. This can be done by observing the atmosphere at additional elevation angles. Therefore, a scanning strategy has been developed in order to maximize the number of weighting functions and thereby enhance the vertical resolution. In this approach, the atmosphere is scanned at elevation angles from 30^0 to 85^0, in increments of 5^0, with the addition of 15^0. There is no restriction on the upper bound of the elevation angles, but the maximum elevation angle is chosen to be 90^0 because the atmosphere is assumed to be vertically stratified. Therefore, measurement at elevation angles greater than 90^0 is considered to be redundant. The lower limit of the elevation angle is set by the

antenna beamwidth i.e., 3-4 degrees and the sidelobe contributions so that there is no contamination of the measured brightness temperature at lower elevation angles due to ground emission. The scanning angles can be seen in Figure 4.2.
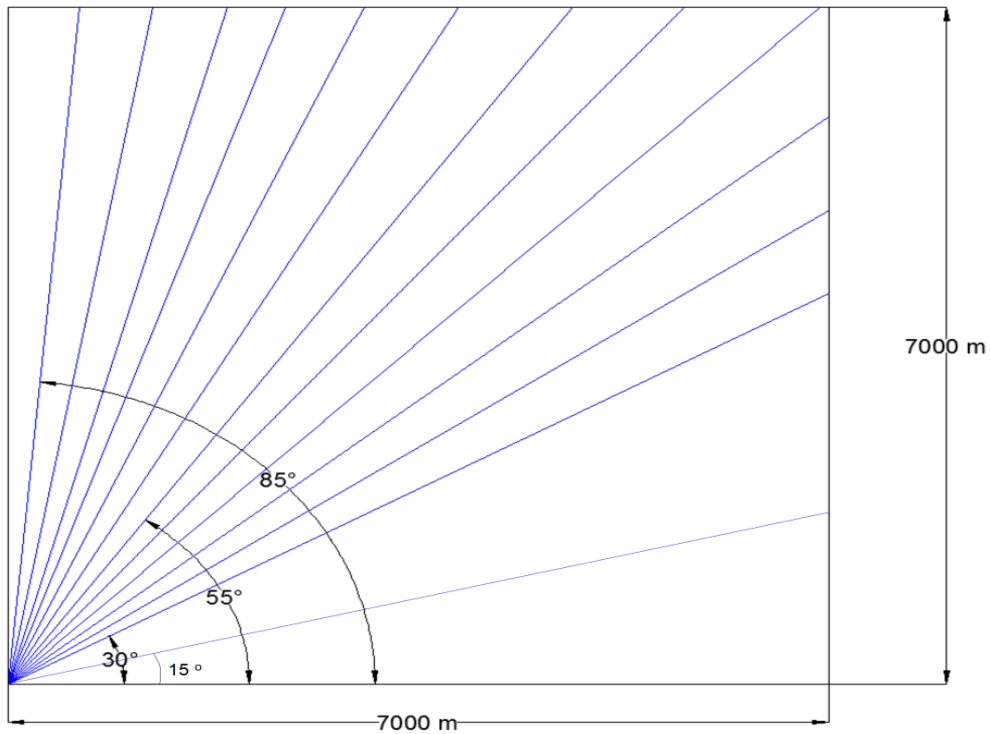
Figure 4.2. Scanning strategy in the vertical plane

Figure 4.3 shows the weighting function for various elevation angles from 15^0 to 85^0 at 22.12 GHz. These weighting functions were computed for the frequency 22.12 GHz.
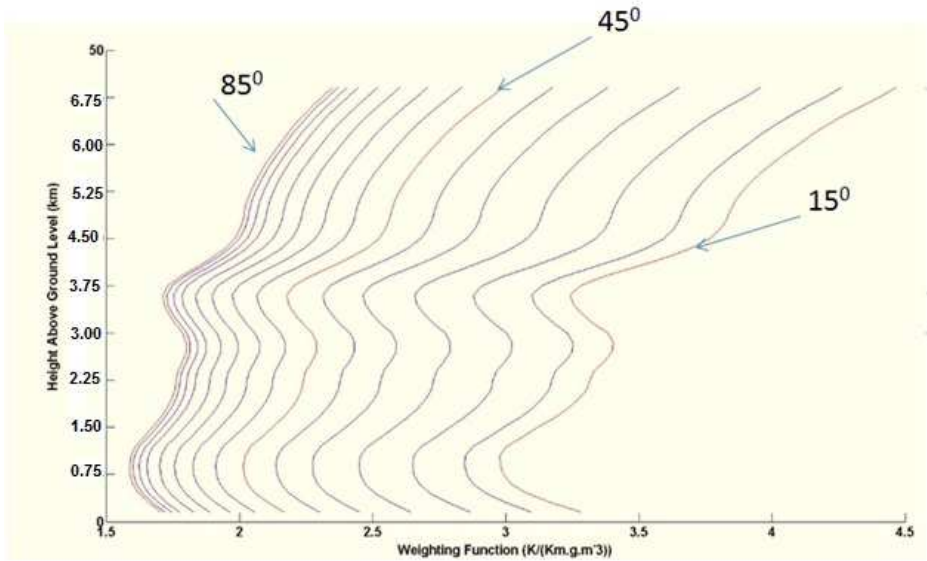
Figure 4.3. The weighting functions for various elevation angles at 22.12 GHz
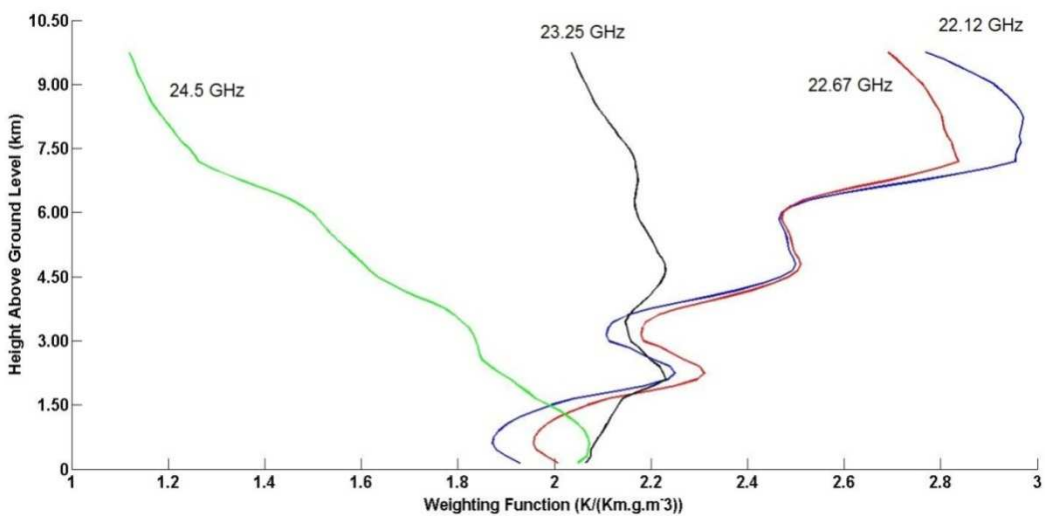
Figure 4.4. Weighting function at the four CMR-H frequencies

4.4 Information Content Analysis

If one weighting function at zenith angle $\theta = \theta_0$ is a linear combination of the others such that $W_{\rho v}(f_1, \theta_1, z) = \sum a_i W_{\rho v}(f_i, \theta_1, z)$ where $i \neq 1$ (4.13)

for all z, then it can be shown that the brightness temperature at frequency f_1 can be calculated

$$T_B(f_1, \theta_1, z) = \sum a_i \, T_B(f_i, \theta_1, z) \text{ where } i \neq 1 \qquad (4.14)$$

Thus those measurements are not useful.

Thus the observation at frequency f_1 introduces no new information.

If a set of coefficients a_i, i=1, 2, …,M (number of measurements) can be found such that

$$\sum_{i=1}^{M} a_i W_{\rho v} \, (f_i, \theta_1, z) = 0 \qquad (4.15)$$

there exists at least one measurement within the data set which can be easily computed from the set of measurements [36]. Basically it means that the measurement is redundant and is not useful in extracting any information about the state vector. Similarly if a weighting function can be predicted within the limits of experimental noise level for all height levels z, the information provided by the corresponding measurement is lost in the noise. Inclusion of this measurement in the forward model provides no new information about the state vector. Similarly if the elevation angle of measurement are increased and the frequency is kept constant and if

$$T_B(f_1, \theta_1, z) = \sum a_i \, T_{AB}(f_1, \theta_i, z) \text{ where } i \neq 1 \text{ where } i \neq 1 \qquad (4.16)$$

then the brightness temperatures T_B can be predicted. Thus linearly independent weighting functions are needed to improve the vertical resolution.

4.4.1 Identifying the Linearly Independent Weighting Functions

An important aspect of the averaging kernel analysis is identifying the linearly independent weighting functions. A method for identifying the independent weighting functions is finding the rank of the weighting functions matrix **W.** If the rank is lower than the matrix dimensions then there is a linear dependency between columns and hence the weighting function are not independent.

$$W = \begin{bmatrix} w_{11} & w_{12} & - & w_{1n} \\ w_{21} & - & - & - \\ - & - & - & - \\ w_{n1} & - & - & w_{nn} \end{bmatrix}$$

The column of the matrix represent the weighting function corresponding to a particular frequency and elevation angle. The rank of the matrix of weighting functions would be equal to the number of linearly independent columns i.e., weighting functions in the matrix [37].

The weighting functions corresponding to the elevation angles 15^0, 55^0, 85^0 are found to be linearly independent and hence would help in optiminzing the vertical resolution. The weighting functions for other elevation angles are linearly dependent, so are redundant and therefore are not useful. The rank of the matrix is found to be 12. Thus there are 12 linearly independent weighting functions corresponding to the 3 elevation angles, that can be used.

4.4.2 Spread values as a function of altitude

As a result of these studies, 12 linearly independent weighting functions corresponding to three elevation angles and four measurement frequencies are chosen. Figure 4.5 shows the spread values using the linearly independent weighting functions in red. Therefore, the vertical resolution that can be achieved by scanning the atmosphere is better than 500 m for the lowest 1 km and better than 750 m for the lowest 2 km of the troposphere. The spread values achieved from the technique are lower than the spread

values of a currently-available inversion technique using a vertically-pointing radiometer, which are shown in blue.
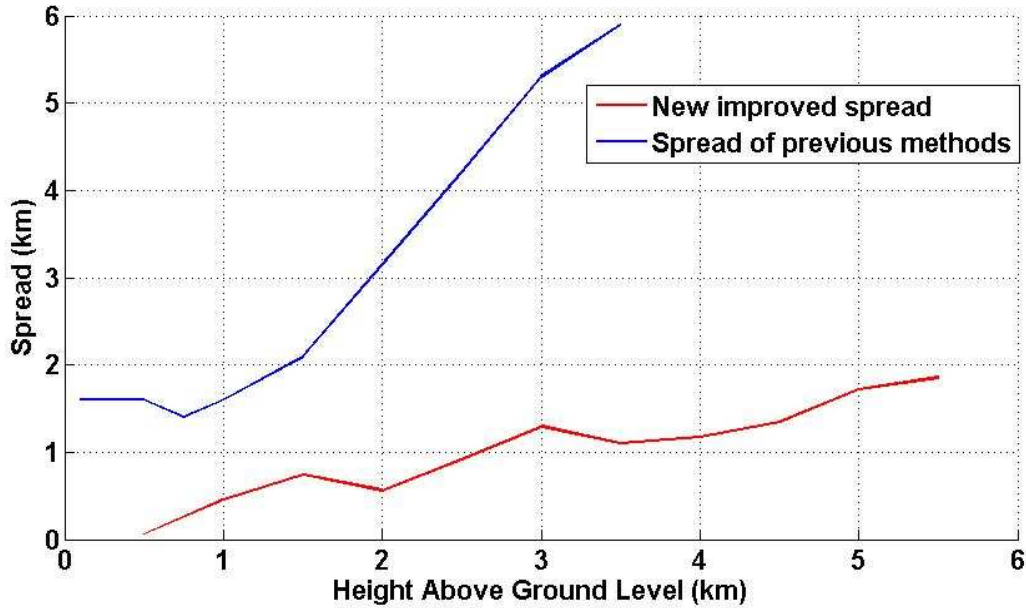
Figure 4.5. Spread for combining weighting functions corresponding to 3 elevation angles

4.5 Conclusion

The Backus-Gilbert method has been used to minimize the spread values. Here it has been shown that spread values decrease with the increase in the number of angular measurements consequently increasing the vertical resolution of water vapor profile. It has also been shown that all the measurements corresponding to the twelve angular are not linearly independent and can't be used for increasing the resolution. The number of angular measurements useful for the minimization of spread was found to be three. The number of independent weighting function varies slightly with change in water vapor

profiles. The number of independent elevation angles varies usually from 3-5 for the

CMR-H specific frequency channels.

Chapter 5

Water Vapor Retrieval and Observation System Simulation Experiment

In this chapter the 1-D variational retrieval technique is discussed. Section 5.1 presents the forward model of the retrieval. The weighting function used for water vapor density retrieval is discussed in section 5.2. Bayesian optimal estimation is discussed in section 5.3. Sections 5.4 - 5.5 discuss the cost function and Gauss-Newton iteration. An observation system simulation experiment (OSSE) was performed using radiosonde data from atmospheric radiation measurement (ARM) site at Southern Great Plains (SGP) and local analysis and prediction system (LAPS) nowcasting data to analyze the capability of the retrieval algorithm to retrieve water vapor density profiles with high vertical resolution.

5.1 Forward Model

The forward model maps the brightness temperature T_B, the measurement vector to the state vector, the water vapor density profile in this case.

$$T_B(f,\theta) = \int_0^H W(f,\theta,z).\rho(z)dz \tag{5.1}$$

$W(f,\theta,z)$ is the weighting function for different elevation angles which has already been described in the previous chapter, $\rho(z)$ is the water vapor profile where z is the height above ground level. In the case of vertically pointing atmospheric brightness temperature

measurements, the lower and upper limits of integration are 0 and H respectively, corresponding to the Earth's surface and top of the troposphere, respectively. The forward model is the radiative transfer equation corresponding to the downwelling emission of the atmosphere. The atmosphere is assumed to be vertically stratified with each layer having thickness dz. The brightness temperature T_B at the frequency f and elevation angle θ is given by

$$T_B(f,\theta) = T_{CMB}e^{-\tau(0,z)} + \int_0^H k_{abs}(z')T(z')e^{-\tau(0,z')\sec(\theta)}dz'(\sec(\theta))$$

(5.2)

Where T_{CMB} is the cosmic background of 2.73 K. k_{abs} is the absorption coefficient at a particular height in Np/km, τ is the optical depth. T is the physical temperature of the atmospheric layer. θ is the angle of elevation.

$$\tau(z) = \int_0^z \kappa(z)dz$$

(5.3)

In order to retrieve the water vapor density profile from the measured brightness temperatures the forward model in equation 5.1 needs to be inverted. The direct inversion will not be possible as W^{-1} is not a square matrix. This is because the number of measurements is less than the number of altitudes at which water vapor density has to be retrieved. This is an ill-posed problem. Consequently optimal estimation is used to estimate the water vapor profile.

5.2 Weighting function

A weighting function is the change in the brightness temperature due to a change in the water vapor density at a particular altitude [38]for unit layer thickness. It is given by

$$W(f,\theta,z) = \lim_{\delta\rho_v,\delta z \to 0} \frac{\delta T_B}{\delta\rho_v \delta z} = \lim_{\delta\rho_v,\delta z \to 0} \frac{\delta T_B}{\delta \bar{B}(T_B)} \cdot \frac{\delta \bar{B}(T_B)}{\delta\rho_v \delta z} \tag{5.4}$$

where $\delta \bar{B}(T_B)$ is resulting change in the modified Planck radiance, $\delta\rho_v$ is the perturbation in atmospheric water vapor, δz is the layer thickness at altitude z and δT_B is the resulting change in brightness temperature [39].

The weighting function is used to characterize the atmosphere at a particular place. The weighting function is usually computed using archived atmospheric data. From 5.4, the weighting function for the water vapor is derived as [39]

$$W_{\rho_v}(f,\theta,z) = \frac{\partial \kappa_a(z)}{\partial \rho_v(z)}[T(z) - T_B(f,z)]e^{-\tau(0,z;f)} \tag{5.5}$$

where $\kappa_a(z)$ is the water vapor absorption coefficient at altitude z, $\rho_v(z)$ is the water vapor density at altitude z, T_B is the brightness temperature, and $T(z)$ is the air temperature at altitude z. Equation 5.5 is modified for radiometer scanning in the vertical plan and is given as [5]

$$W_{\rho_v}(f,\theta,z) = \frac{\partial \kappa_a(z)}{\partial \rho_v(z)}[T(z) - T_B(f,\theta,z)]e^{-\tau(0,z;\theta;f)\sec(\theta)} \tag{5.6}$$

where θ is the scanning angle.

5.3 Bayesian Optimal Estimation

The discrete form of the weighting function W is an m x n matrix for each elevation angle scanned by a radiometer, where m is the number of measurements are

taken and n is the number of altitudes at which the water vapor density is to be retrieved. Since the inversion of the measurements to retrieve geophysical quantities like water vapor and temperature requires finding the inverse of W, the solution is under-constrained as the number of measurements (m) is less than the number of vertical heights (n) at which the quantity is to be retrieved, which is nearly always the case with microwave radiometry. This problem can be taken care of by limiting the set of admissible solutions to a set of physically realizable solutions. This is done by including *a-priori* knowledge. In this regard, the Bayesian Optimal Estimation technique [16] was chosen to retrieve a water vapor density profile using the brightness temperatures measured at the four frequencies of the CMR-H and various elevation angles. Bayes' theorem provides a methodology to invert the forward model and compute an *a-posteriori* probability density function (pdf) by updating the a-priori with the measurement.

$$\hat{\rho}_v = \rho_{v,a} + S_{\rho,a} W^T (W S_{\rho,a} W^T + S_{TB})^{-1} (T_B - W\rho_{v,a}) \qquad (5.7)$$

where ρ_v is the water vapor density profile to be retrieved, $\rho_{v,a}$ is the *a−priori* profile, $S_{\rho_{v,a}}$ is the error covariance matrix of the *a−priori* water vapor profile, S_{TB} is the error covariance matrix corresponding to the measured brightness temperatures, and W is the weighting function matrix. The measurement errors are assumed to be independent of each other.

5.4 Minimizing Cost Function and Gauss-Newton Method

Assuming Gaussian probability distribution of observational errors the inversion problem can be presented as a problem of minimizing a cost function. The water vapor

profile retrieved is non-unique. Therefore, the retrieval is performed by selecting a water

vapor profile that minimizes a cost function in the form of

$$J(\rho_v) = \left[T_B - W \cdot \rho_v \right]^T S_{T_B}^{-1} \left[T_B - W \cdot \rho_v \right] + \left[\rho_v - \rho_{v,a} \right]^T S_{\rho v}^{-1} \left[\rho_v - \rho_{v,a} \right] \qquad (5.8)$$

where the forward model is represented by $W \cdot \rho_v$

The minimization of the cost function can be done numerically, by using the water vapor

density profiles computed using the iterative Gauss-Newton method [17]

$$\rho_{i+1} = \rho_{va} + S_{\rho v_a} W_i^T (W_i S_{\rho v_a} W_i^T + S_{T_B})^{-1} [T_B - W_i \rho_{vi} + W_i (\rho_i - \rho_a)] \qquad (5.9)$$

where ρ_a is *a-priori* profile. Equation 5.9 is used to compute the water vapor profile at

i*th* iteration. The i*th* profile is used to update the profile in the equation 5.8 which is used

to compute the value of the cost function. The water vapor profile from each iteration in

equation 5.9 is again used to recomputed W, using equation 5.6 which in turn is used in

equation 5.9. This process goes on until the minimum value of the cost function J is

reached.

Usually the iteration is started with ρ_{va} as ρ_a .The errors in the *a−priori* water

vapor density and measured brightness temperatures are modeled as covariance matrices

S ρ_v and S$_{TB}$, respectively. The covariance of the observation vector T$_B$(with dimension

m) is an m x m matrix. The co-variance of the *a-priori* water vapor density $\rho_{v,a}$ (with

dimension n) is a n x n matrix. The main diagonal of each covariance matrix contains a

set of variances of each variable; the off-diagonal elements contain cross-covariances

between each pair of variables. A reasonable *a-priori* of water vapor would have adjacent

vertical levels correlated [17]. So a covariance matrix for *a-priori* error is based on Markov process. The error covariance matrix of the *a-priori* water vapor density S $\rho_{v,a}$ is

$$S_{\rho v}(i, j) = \sigma_a^2 e^{\frac{-|i-j|\delta z}{h}}$$ (5.10)

where σ_a is the standard deviation of the a-priori water vapor densities in gm/m^3, h is the length scale, empirically estimated as 6 km, and dz is the altitude spacing.

Here the departure of the water vapor from the mean $\delta\rho_{i+1}$ at level i+1 is related to $\delta\rho_i$ at level i by the relation

$\delta\rho_{i+1}=\beta.\delta\rho_i+\xi_i$ (5.11)

The regression coefficient β is a constant between 0 and 1 and ξ_i is a Gaussian random variable uncorrelated with $\delta\rho_i$ and has a constant variance, σ^2_ξ.

Variance of $\delta\rho$ tends to $\sigma^2_\xi/(1-\beta^2)$

$\sigma^2_\xi = \sigma_a^2(1-\beta^2)$ (5.12)

σ_a is found to be 0.8758 g/m^3

The value of σ_a changes from place to place. The above mentioned value of σ_a was calculated for SGP site. Additionally the uncertainty in the brightness temperatures error covariance matrix, S_{TB}, is represented by the main diagonal elements of the error covariance matrix.

5.5 Observation System Simulation Experiment

5.5.1 Definition

Observation System Simulation Experiment (OSSE) are usually designed and conducted to use data assimilation techniques to investigate potential impact and use of prospective observing systems. They may also be used to investigate current observational and data assimilation systems (DAS) by testing the impact of new observations on them [40]. In OSSE simulated observations are provided as input to a data assimilation system. These observational values are then ingested into DAS as corresponding real observations. The simulations of analyses and subsequent forecasts are then produced for several experiments, with each considering a distinct set of observations. The analysis and forecast products are then compared to evaluate the impacts of various systems considered. The OSSE performed for this study is presented in the following subsections.

5.5.2 OSSE for 1-D Water Vapor Retrieval

The OSSE was performed using data sets from 2 different sources of data. The 1st data set was from radiosondes from the radiosonde launch site of the atmospheric radiation measurement (ARM) Southern Great Plains (SGP) site in Billings, OK, USA.The 2nd data set was taken from the local analysis and prediction system (LAPS) 1-D outputs for Denver, CO. Results of OSSE for 1-D water vapor retrieval have been presented in the following sub-sections.

5.5.3 OSSE using Radiosonde Data from SGP Site

The water vapor and temperature profiles information were used to compute the synthetic brightness temperature. The computed brightness temperatures were inverted to retrieve water vapor profile. The retrieved and actual profiles were compared. Here radiosonde data from two separate days i.e., 08-June-2007 and 11-June-2007,have been used for the study. The simulated brightness temperatures from 3 elevation angles were used. The elevation angles were 30^0,55^0 and 85^0. The results of the retrieval are presented and discussed here.
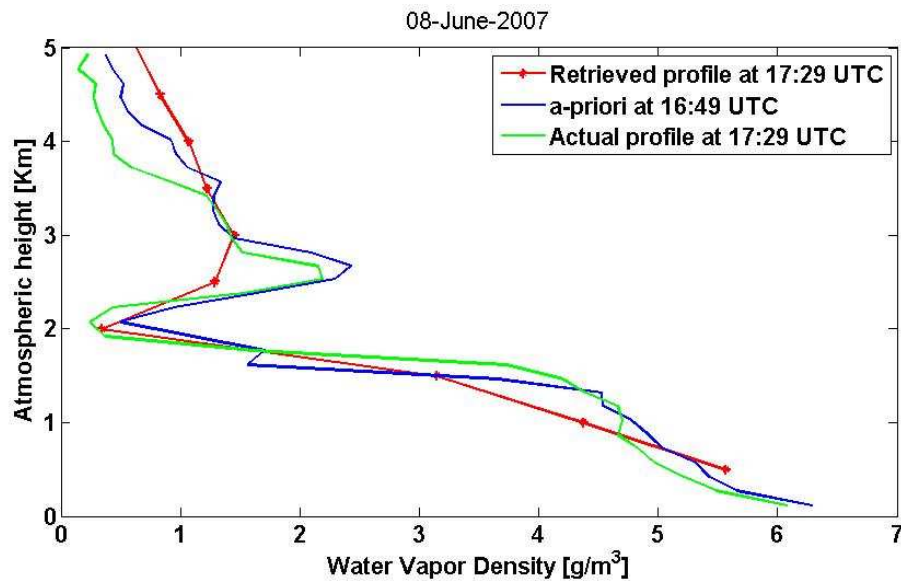

Figure 5.1. Comparison between a-priori, retrieved profile and original profile for on 8-June-2007

It can be seen in the Figure 5.1 that the retrieved profile is somewhat similar to the actual profile for most of the lower 2 km of the troposphere. The difference in the retrieved water vapor profile and actual profile for the first 2 km of the lower troposphere varies from 0 to 1.3 g/m^3. It shows the sharp inversion in the water vapor profile around 2 km AGL. The retrieved profile deviates from the actual profile for the range 2.3 – 3.0 km AGL and then follows the actual profile above 3 km to a certain extent. The difference in the retrieved water vapor profile and actual profile for the altitude range 2 – 5 km varies from 0 – 1 g/m^3.
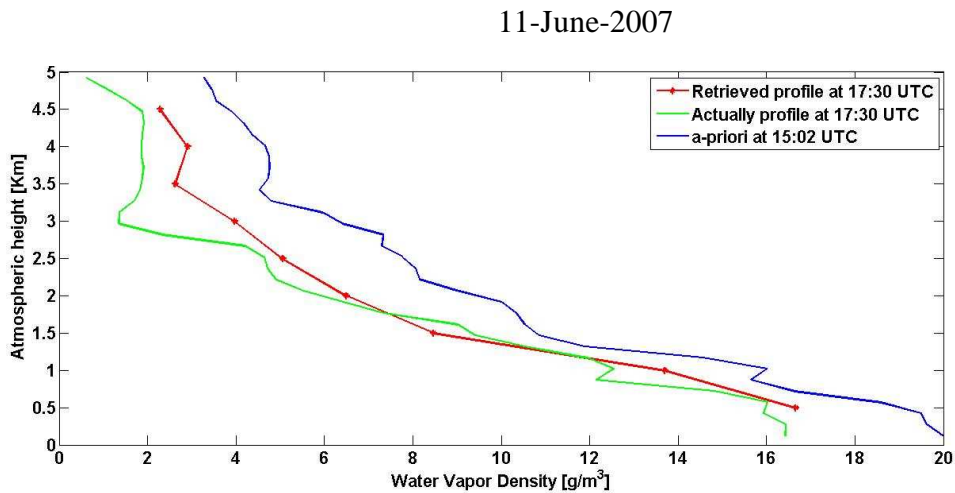
11-June-2007

Figure 5.2. Comparison between a-priori, retrieved profile and original profile for 11-June-2007

The Figure 5.2 shows that retrieved profile follows the actual profile closely from ground until 2.5 km AGL. The difference between the actual profile and retrieved profile varies from 0 – 0.75 g/m^3 from ground till 2.5 km AGL. Above that the water vapor profile deviates from the actual profile and doesn't show the inversion at around 3 km but the retrieved profile follows the actual profile. The retrieved profile differs from the

71

actual profile in the range 0.2 - 1 g/m^3. In both the above mentioned cases it can be noted that the retrieved profile is similar to the actual profile for most of the 2.5 km of the lower troposphere.

5.5.4 OSSE using Local Analysis and Prediction System

Forecast applications branch (FAB) developed the Local Analysis and Prediction System (LAPS) for data assimilation, nowcasting, and initialization of numerical prediction models [41]. LAPS makes use of a wide variety of local, national, and global datasets. The data from ground measurement systems, Doppler radars, satellites, wind and temperature profilers, radiometric profilers, as well as aircraft are fed every hour into a three-dimensional grid of area 1040 km by 1240 km. The size of each grid size is 10 km x 10 km. There are 105 x 105 such grids cells. The models, initialized with LAPS output, are run to provide short-term forecasts. LAPS has a vertical resolution of 50 hPa. The height above ground level corresponding to 1100 and 100 hPa are divided into 21 pressure levels. It has a temporal resolution of 1 hour so the forecast data is available every one hour. So water vapor and temperature profiles are available every hour. LAPS is run in real-time for a domain centered on the Denver, CO Weather Forecast Office.

LAPS is being used by federal and state agencies (National Weather Service, and the United States Air Force), private sector, universities in the US like Univ. of Oklahoma ("OLAPS"), Univ. of North Dakota, and Univ. of Hawaii's Mauna Kea Weather Center, and international organizations like Taiwan's Central Weather Bureau.

LAPS has two components i.e., analysis and prediction. The analysis component has three options, "traditional" LAPS, Space-Time Mesoscale Analysis System (STMAS), and Gridded Statistical Interpolation (GSI). The prediction component is configured using models like MM5 and WRF. The products of LAPS are used to initialize mesoscale forecast models like WRF, MM5 and vice-versa for both analyses and prediction purpose. Here LAPS product has been used for OSSE to test it use in future as *a-priori* thus reducing the dependence on radiosondes which has a low temporal resolution.

The prediction component has been used in this case. Figure 5.3 shows the results of OSSE performed on the LAPS forecast data. Here it can be seen that the absolute value of difference between the retrieved water vapor density profile and the forecast profile varies from 6 to 15 % for most of the lower 3 km of the troposphere.
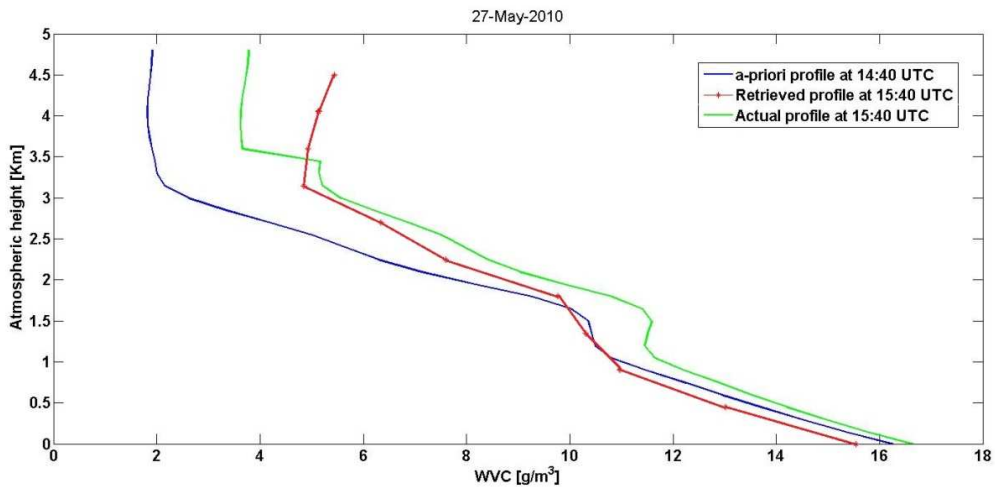
Figure 5.3. Comparison between a-priori, retrieved and forecast profile

5.6 Conclusion

Variational retrieval technique has been used to retrieve water vapor density profiles with high vertical resolution. The synthetic measurements at 3 elevation angles

were used for the variational retrieval. It has been shown using the OSSE that the water vapor retrievals are similar to the actual or forecast profiles for most part of the lower troposphere. It can be noted that the retrieved profile vary from the actual profile by a maximum amount of 1.5 g/m^3 for most of the lower 2.5 km of the troposphere. It can also be seen that LAPS output can be used as a-priori for the retrieval technique, as the forecast model produces output every 1 hour.

Chapter 6

Conclusion and Future work

6.1 Conclusion

The results of retrievals using brightness temperature measurements from a network of Compact Microwave Radiometer for Humidity profiling during the METAWAVE experiment demonstrated the ability of the network to retrieve 3-D water vapor with high resolution and accuracy of better than 15-20%. The retrieval technique achieves a vertical and horizontal resolution of approximately 500 meters and a temporal resolution of approximately 10 minutes. The comparisons between retrievals from CMR-H network measured brightness temperatures and passive optical measurements from the MODIS and MERIS polar-orbiting satellite instruments show good potential to correct Interferometric Synthetic Aperture Radar (InSAR) imagery for variations in wet-tropospheric delay. This can be verified by a long time sequence of SAR acquisitions over Rome, Italy which can be exploited using the permanent scatters technique [27]to potentially provide path delay estimates. These estimates could be compared to the CMR-H products. Also it is clear that MERIS data and CMR-H network retrievals agree well under moderately humid conditions and can be used to retrieve columnar water vapor content with a difference of 0.1 to 0.75 mm for geographically co-located pixels. These results demonstrate the capability of the CMR-H network to retrieve IWV with high

spatial and temporal resolution, while maintaining quality comparable to that of mature water vapor products. More comparisons need to be performed in order to validate the 3-D water vapor density retrievals from CMR-H network brightness temperature measurements and to determine definitively whether or not such retrievals can be used to correct InSAR images for variations in wet-tropospheric path delay.

As already discussed the water vapor retrieved, from the CMR-H network has a vertical and horizontal resolution of around 500 meters but for detecting the planetary boundary layer (PBL) and the water vapor profile in the PBL a vertical resolution of better than 500 meters would be required. This is because the PBL height typically varies from 100 m to 3000 m. Usually radiosondes have a vertical resolution of tens of meters which is a big advantage in finding the boundary layer height but have a horizontal resolution of about 100 to 300 km as well as a temporal resolution of about 6 hours. The horizontal and temporal resolution limit the capability of radiosondes to characterize the PBL. Therefore a new technique has been used to test the ability of the CMR-H to retrieve water vapor profile with high vertical resolution which in turn will help in approximately determining the PBL height. The Backus-Gilbert method of using multiple weighting functions has been used here. Usually state-of-art techniques used to get a good vertical resolution from a given data set, increase the sensitivity of the retrieved profiles to random noise [33]. Therefore a tradeoff between resolution and its stability to variation in noise exists. This can be taken care of in the Backus-Gilbert technique by minimizing a linear combination of vertical resolution and noise. Thus the vertical resolution is increased, while estimating the sensitivity of resolution to noise. The results of spreads of averaging kernels have shown that the vertical resolution of water vapor

profile can be increased using a combination of linearly independent weighting functions. The linearly independent weighting functions correspond to 3 or 4 elevation angles from 0 to 90^0, depending on the water vapor profile used. The elevation angles were limited between 0 to 90^0 as the atmosphere was considered vertically stratified. The ability of the retrieval algorithm to retrieve water vapor with high vertical resolution was tested by performing an OSSE. OSSE was performed using data sets from two different sources like radiosondes from SGP site and forecast data from LAPS. The OSSE has proved that water vapor density profile can be retrieved with good accuracy using linearly independent weighting functions and corresponding measurements.

6.2 Future Work

Some recommendations for future work are as follows:

1) A field deployment of the CMR-H network in conjunction with other water vapor retrieving or in-situ measurement instruments (including a Radiometrics radiometer, Raman lidar, radiosondes, etc.) observing the same volume of the atmosphere at the same time. The results from the CMR-H network could be validated through comparison with measurements from other instruments. The best site for this purpose would be the SGP site of ARM in Billings, Oklahoma which has a large number of such instruments. . The data collected by the radiosondes can be used as *a-priori* for the CMR-H network and the data retrieved using other instruments like Raman lidar can be used to compare with CMR-H retrievals. One important reason for choosing the SGP site of ARM is that Oklahoma is known for severe weather like tornados, rain and hail storm

2) The future work would also aim at increasing the accuracy of output of the Kalman filter. Presently a non-linear Kalman filter is used to keep track of the a-posteriori 3-D water vapor profile. The change in accuracy of the a-posteriori output due to use of a linear Kalman filter is to be included in the future study.

3) The tradeoff between vertical resolution and sensitivity of algorithm to noise according to Backus-Gilbert method is to be investigated.

4) Future work can also include the use of the LAPS output as a-priori instead of a radiosonde data thus decreasing the dependence on radiosondes. LAPS outputs are available as 3-D water vapor fields which would increase the accuracy of the retrieval. The 3-D water vapor field would provide a better a-priori. LAPS output is available every 1 hour thus increasing the accuracy of temporal resolution output of the 3-D water vapor field.

Bibliography

[1] R. B. Stull, *An Introduction to Boundary Layer Meteorology*.: Kluwer Academic, 1988.

[2] *Glossary of Meteorology*.: American Meteorological Society,2nd ed., 2000.

[3] A. V. Engeln and J. Teixeira, *Determining the Planetary Boundary Layer Height from Radio Occultation Data*., 2004.

[4] http://apollo.lsc.vsc.edu/classes/met455/notes/section1/1.html.

[5] F. Iturbide-Sanchez, S. C. Reising, and S. Padmanabhan, "A Miniaturized Spectrometer Radiometer Based on MMIC Technology for Tropospheric Water Vapor Profiling," *IEEE Trans. Geosci. Remote Sensing*, vol. 44, no. 7, pp. 2181-2193, Jul. 2007.

[6] S. Padmanabhan, S. C. Reising, J. Vivekanandan, and F. Iturbide-Sanchez, "Retrieval of atmospheric water vapor density with fine spatial resolution using three-dimensional tomographic inversion of microwave brightness temperatures measured by a network of scanning compact radiometers," *IEEE Trans. Geosci. Remote Sensing*, vol. 7, no. 11, pp. 3708-3721, Nov. 2009.

[7] C. N. Banwell, *Fundamentals of Molecular Spectroscopy*. New York: McGraw-Hill, 1972, p. 338.

[8] W. Gordy and R. L. Cook, *Microwave Molecular Spectra*. New York: Wiley, 1984, pp. 37-61.

[9] C. H. Townes and A. L. Schawlow, *Microwave Spectroscopy*. New York: McGraw-Hill, 1955, pp. 336-338.

[10] G. L. Stephens, *Remote Sensing of the Lower Atmosphere: An Introduction*. New York: Oxford University Press, 1994.

[11] F. T. Ulaby, R. K. Moore, and A. K. Fung, *Microwave Remote Sensing*. London, UK: Addison-Wesley, 1981, p. 372.

[12] G. E. Backus and F. E. Gilbert, "Uniqueness in the inversion of inaccurate gross earth data," *Phil. Trans. Roy. Soc. London*, vol. A266, pp. 123-192, 1970.

[13] K. A. Emanuel et al., "Report of the first prospectus development team of the US weather research program to NOAA and the NSF," *Bull. Amer. Meteor. Soc.*, vol. 76, pp. 1194-1208, 1995.

[14] S. K. Park and K. K. Droegemeier, "Sensitivity analyis of a moist 1D Eulerian cloud model using automatic differentiation," *Mon. Wea. rev.*, vol. 127, no. 9, pp. 2180-2196, 1999.

[15] S. K. Park and K. K. Droegemeier, "Sensitivity analysis of a 3D convective storm: Implications for variational data assimilation and forecast error," *Mon. Wea. Rev.*, vol. 128, no. 1, pp. 140-149, 2000.

[16] T. J. Hewison, "1D-VAR Retrieval of Temperature and Humidity Profiles from a Ground-based Microwave Radiometer," *IEEE Trans. Geosci. Remote Sens.*, vol. 45, no. 7, pp. 2163-2168, Jul. 2007.

[17] C. D. Rodgers, *Inverse Methods for Atmoshperic Sounding: Theory and Practice*. Singapore: World Scientific , 2000.

[18] A. V. Bosisio and G. Drufuca, "Retrieval of two-dimensional absorption coefficient structure from a scanning radiometer at 23.8 GHz," *Radio Sci.*, vol. 38, no. 3, p. 8038, 2003.

[19] G. H. Golub and C. F. Van Loan, *Matrix Computations*. Baltimore, MD: Johns Hopkins University Press, 1996, pp. 70-71 and 73.

[20] P. W. Rosenkranz, "Erratum: 'Water vapor microwave continuum absorption: A comparison of measurements and models'," *Radio Sci.*, vol. 34, no. 4, p. 1025, Jul./Aug. 1999.

[21] P. W. Rosenkranz, "Water vapor microwave continuum absorption: A comparison of measurements and models," *Radio Sci.*, vol. 33, no. 4, pp. 919-928, Jul./Aug. 1998.

[22] J. C. Liljegren, S.-A. Boukabara, K. Cady-Pereira, and S. A. Clough, "The effect of the half-width of the 22-GHz water vapor line on retrievals of temperature and water vapor profiles with a 12-channel microwave radiometer," *IEEE Trans. Geosci. Remote Sens.*, vol. 43, no. 5, pp. 1102-1108, May 2005.

[23] R. J. Hill, "Water vapor-absorption line shape comparison using the 22-GHz line: The Van Vleck-Weisskopf shape affirmed," *Radio Science*, vol. 21, pp. 447-451, May-June 1986.

[24] T. J. Hewison and C. Gaffard, "Combining Data From Ground-Based Microwave Radiometers and Other Instruments in Temperature and Humidity Profiles Retrievals," in *Proceedings of TECO-2006 - WMO*, Geneva, Switzerland, 4-6 December 2006.

[25] D. Massonnet and K. L. Feigl, "Radar interferometry and its application to changes in the earth's surface," *Rev. Geophys.*, vol. 36, no. 4, pp. 441-500, 1998.

[26] H. A. Zebker, P. A. Rosen, and S. Hensley, "Atmospheric effects in interferometric synthetic aperture radar surface deformation and topographic maps," *J. Geophys. Res.*, vol. 102, no. B4, pp. 7547-7563, 1997.

[27] A. Ferretti, C. Prati, and F. Rocca, "Permanent scatterers in SAR interferometry," *IEEE Trans. Geosci. Remote Sens.*, vol. 39, no. 1, pp. 8-20, 2001.

[28] B.-C. Gao and Y. J. Kaufman, "Water vapor retrievals using Moderate Resolution Imaging Spectroradiometer (MODIS) near-infrared channels," *J. Geophys. Res.*, vol. 108, p. 4389, 2003.

[29] ESA, *MERIS product Handbook.*, 2002.

[30] N. Pierdicca et al., "Atmospheric water-vapour effects on spaceborne Interferometric SAR imaging: data synergy and comparison with ground-based measurements and meteorological model simulations at urban scale," in *Proceedings of EuCAP*, Berlin, Germany, 23-27 March 2009.

[31] R. Lang, S. Casadio, A. N. Maurellis, and M. G. Lawrence, "Evaluation of the GOME water vapor climatology 1995–2002," *J. Geophys. Res.*, vol. 112, no. D17110, 2007.

[32] Wikipedia. [Online]. http://en.wikipedia.org/wiki/Inversion_%28meteorology%29

[33] B. J. Conrath, "Vertical resolution of temperature profiles obtained from remote

radiation measurements," *J. Atmos. Sci.*, vol. 29, pp. 1262-1271, 1972.

[34] D. G. Long, "Spatial resolution enhancement of Cassini Titan Radar mapper data," in *Proceedings of Radar Conference*, 2009.

[35] C. D. Rodgers, "The vertical resolution of remotely sounded temperature profiles with a priori statistics," *J. Atmos. Sci.*, vol. 33, pp. 707-709, 1976.

[36] T. M. Scheve and C. T. Swift, "Profiling atmospheric water vapor with a K-band spectral radiometer," *IEEE Trans. Geosci. Remote Sensing*, vol. 37, pp. 1719-1729, May 1999.

[37] S. H. Friedberg, *Linear algebra*. Upper Saddle River, NJ: Prentice Hall, 1997.

[38] S. Padmanabhan, "Three-Dimensional Water Vapor Retrieval Using a Scanning Network of Compact Microwave Radiometers," Colorado State University, Fort Collins, Ph. D dissertation 2008.

[39] J. A. Schroeder and E. R. Westwater, "Guide to microwave weighting function calculations," U.S. Dept. of Commerce, National Oceanic and Atmospheric Administration, Environmental Research Laboratories, Wave Propagation Laboratory, July 1992.

[40] M. MASUTANI et al., "OBSERVING SYSTEM SIMULATION EXPERIMENTS," 2009.

[41] NOAA. Local Analysis and Prediction System. [Online]. http://laps.noaa.gov

[42] R. Bennartz and J. Fischer, "Retrieval of columnar water vapour over land from backscattered solar radiation using the Medium Resolution Imaging Spectrometer," *Rem. Sens. Environ.*, vol. 78, no. 3, pp. 274-283, 2001.

[43] NOAA. Rapid Update Cycle. [Online]. http://ruc.noaa.gov

[44] U. Löhnert, S. Crewell, and C. Simmer, "An integrated approach toward retrieving physically consistent profiles of temperature, humidty, and cloud liquid water," *J. Appl. meteor.*, vol. 43, pp. 1295-1307, 2004.

[45] C. S. Ruf and C. T. Swift, "Atmospheric profiling of water vapor density with a 20.5-23.5 GHz autocorrelation radiometer," *J. Atmos. and Oceanic Technol.*, vol. 5, pp. 539-546, 1988.

[46] M. A. Janssen, *Introduction to Passive Remote Sensing*. New York: Wiley-Interscience, 1993.